Negative microfilm Mic 61–1825
received from university

VAN PUTTEN, Jr., James Dyke. DETERMINATION OF THE Λ° DECAY PARAMETER, α.

University of Michigan, Ph.D., 1961
Physics, nuclear

University Microfilms, Inc., Ann Arbor, Michigan

DETERMINATION OF THE Λ^0 DECAY ASYMMETRY, α

by
James Dyke van Putten, Jr.

A dissertation submitted in partial fulfillment
of the requirements for the degree of
Doctor of Philosophy in the
University of Michigan
1960

Doctoral Committee:

Professor Donald A. Glaser, Chairman
Professor Kenneth M. Case
Assistant Professor Clifford T. Coffin
Assistant Professor Andrejs Olte
Associate Professor George H. Trilling

TABLE OF CONTENTS

		Page
LIST OF ILLUSTRATIONS		iv
LIST OF SYMBOLS		v
I.	INTRODUCTION	1
II.	EXPERIMENTAL EQUIPMENT	3
	2.1 The Xenon Bubble Chamber	3
	2.2 The Scanning Equipment	9
	2.3 The Measuring Equipment	9
III.	DATA REDUCTION	11
	3.1 Scanning and Measurement	11
	3.2 Analysis of Events	14
	3.3 Detection of Proton Nucler Scatterings	22
IV.	DETERMINATION OF PROTON POLARIZATION	25
	4.1 Polarization Scattering	25
	4.2 Analysing Strength of Xenon	26
	4.3 Energy Loss on Scattering	31
V.	DESCRIPTION OF α ANALYSIS TECHNIQUE	35
	5.1 Description of Λ^0 Decay	35
	5.2 Realization of Transverse Polarization of the Proton	38
	5.3 The Total Probability of Finding a Given Event Configuration	40
VI.	EXPERIMENTAL RESULTS	42
	6.1 General Properties of the Sample	42
	6.2 Determination of αP	43
	6.3 Determination of α	44

TABLE OF CONTENTS CONT'D

		Page
6.4	Discussion of Results	51
VII.	PROPOSAL FOR NEW EXPERIMENT	56
7.1	Basic Considerations	56
7.2	Polarization Requirement	57
7.3	Λ^0 Momentum Requirement	58
7.4	Requirement on Energy Loss Measurement	58
7.5	Analysing Strength Requirement	61
7.6	Possible Experimental Methods for Determining the Λ^0 Decay Parameters	61
VIII.	APPENDICES	64
8.1	Derivation of the Angular Distribution of Polarization of the Protons from Λ^0 Hyperons	64
8.2	An Analysis Theorem	71
8.3	Construction of $\hat{k}_p^*$	74
LIST OF REFERENCES		78

LIST OF ILLUSTRATIONS

Page

Figure

1. Bubble Chamber Cross Section..... 4
2. Schematic of Bubble Chamber Electronics..... 7
3. Distribution of Coplanarity Angle..... 17
4. Distribution of ξ 19
5. Θ_{RMS} as a Function of Energy..... 23
6. Analysing Strength for Several Elements at 138 MeV..... 27
7. Analysing Strength for Xenon (Low Energy)..... 29
8. Analysing Strength for Xenon (High Energy)..... 30
9. ΔE Distribution..... 33
10. Coordinate System..... 36
11. $|S(\theta,E)|$ Distribution..... 45
12. Distribution of Proton Energy at Scattering..... 46
13. Λ^0 Momentum Distributions..... 48
14. ν^* Distribution..... 49
15. Likelihood Function Plot..... 52
16. ϕ Distribution..... 54
17. $\frac{d\sigma}{d\Omega} \cdot S(\theta,E)$ as a Function of θ 59
18. Coordinate System..... 75

LIST OF SYMBOLS

$\hat{k}_B$ - The π^- beam direction.

$\hat{k}_\Lambda$ - The Λ^0 flight direction.

$\vec{k}_p$ - The proton momentum at decay.

$\hat{k}_p$ - The proton direction at decay.

$\vec{k}_\pi$ - The decay pion momentum at the Λ^0 decay.

$\hat{k}_\pi$ - The decay pion direction at the Λ^0 decay.

E_π - The decay pion energy in the laboratory system at the Λ^0 decay.

$\hat{k}_i$ - The proton direction immediately before scattering.

$\hat{k}_f$ - The proton direction immediately after the scattering.

$\hat{n}$ - The normal to the scattering plane.

θ - The scattering angle.

E - The energy of the proton at the scattering.

ϕ - The azimuthal scattering angle.

β_Λ - The velocity of the Λ^0 in units of the velocity of light.

P - The polarization of the Λ^0 sample.

$\vec{V}$ - The polarization of the proton

$S(\theta,E)$ - The analysing strength

χ^* - The angle between the proton and the $\hat{z}$ axis in the Λ^0 rest frame.

ν^* - The azimuthal decay angle.

$\hat{k}_p^*$ - The direction of the proton in the Λ^0 rest frame.

α, β, γ - The Λ^0 decay parameters.

I. INTRODUCTION

The decay of a spin $\frac{1}{2}$ particle into a spin $\frac{1}{2}$ particle and a spin zero particle can be described in terms of the complex amplitudes of the S and P waves in the final state. Let A be the amplitude of the S wave; and B, the amplitude of the P wave. As shown in Appendix 8.1, α, can be defined in the following manner:

$$\alpha = \frac{2\,\mathrm{Re}\,A^{*}B}{A^{2}+B^{2}} \quad , \quad 0 \leq |\alpha| \leq 1 \ .$$

α is the asymmetry parameter in decay of a spin $\frac{1}{2}$ particle. The magnitude of α is a measure of the parity mixing in the decay.

One way to determine whether or not parity is conserved in the decay of the Λ° hyperon, a spin $\frac{1}{2}$ particle[1], is to observe if there is any asymmetry in the distribution of the decay proton momentum with respect to the spin of the Λ°. This distribution is described mathematically by

$$f(x^{*}) = \tfrac{1}{2}\left(1 - \alpha P \cos x^{*}\right)$$

where x^{*} is the angle between the Λ° spin direction and the proton direction in the Λ° rest frame, and P is the polarization of the Λ°. Parity is thought to be conserved in the Λ° production process[2], a strong interaction; thus the Λ° polarization is always perpendicular to the plane containing the incoming π^{-} meson and the outgoing Λ°

hyperon. The direction of the polarization of the Λ^0 can be defined by:

$$\frac{\hat{k}_B \times \hat{k}_\Lambda}{|\hat{k}_B \times \hat{k}_\Lambda|}$$

where $\hat{k}_B$ is the direction of the incoming π^- meson, and $\hat{k}_\Lambda$ is the direction of the outgoing Λ^0 hyperon.

The observation of parity nonconservation in the Λ^0 decay process[3] raised the interesting question of the magnitude and sign of α. However, as only the product αP could be deduced from the distribution

$$f(x^*) = \frac{1}{2}(1 - \alpha P \cos x^*)$$

another experiment was necessary.

Lee and Yang[4] have pointed out a clever way to express the polarization of the nucleons from decaying hyperons in terms of the parameter α and the polarization of the Λ^0. In the present experiment the decay mode

$$\Lambda^0 \longrightarrow P + \pi^-$$

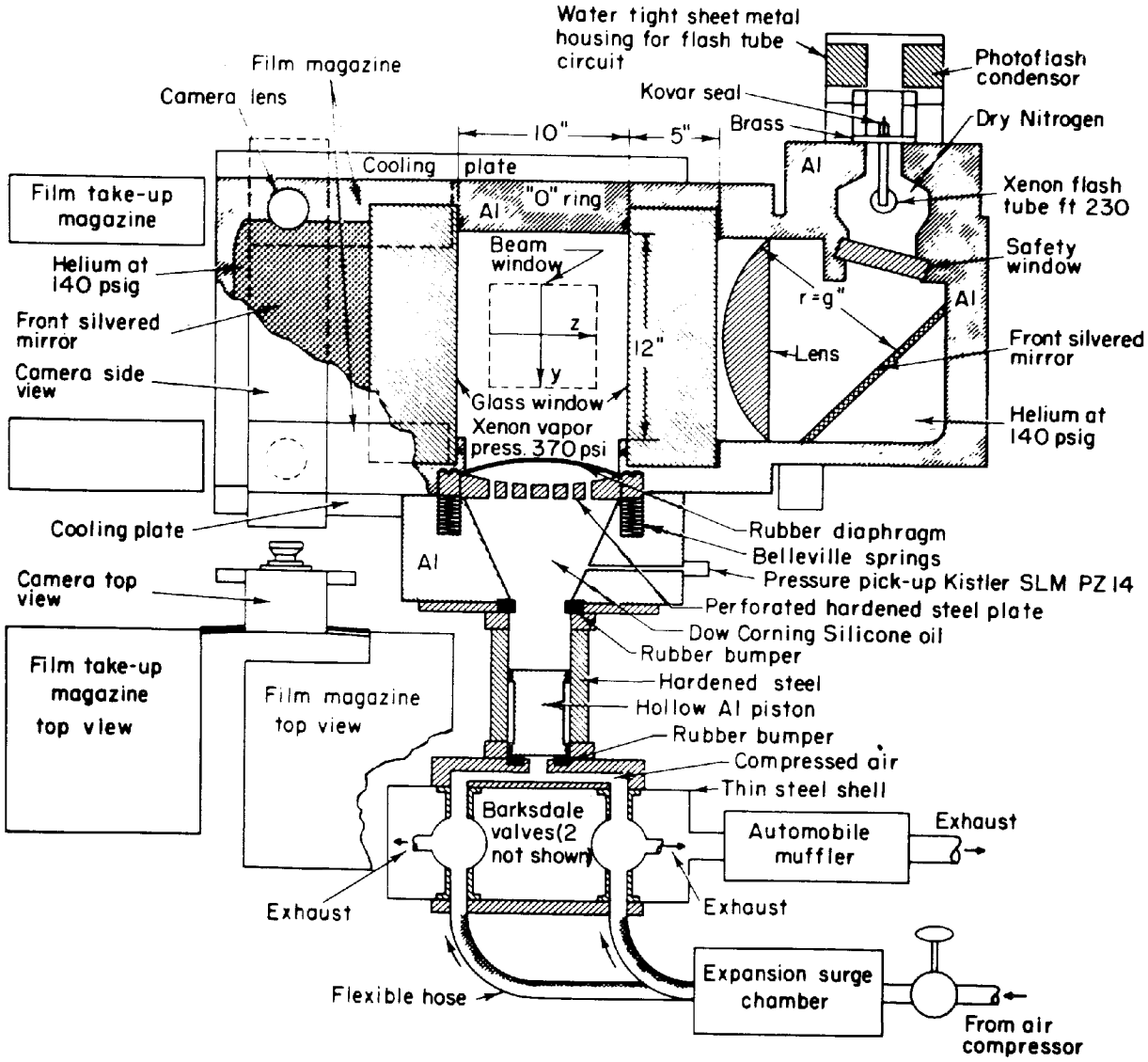
was observed in a Xenon Bubble Chamber and the proton polarization determined by studying the asymmetric scattering of the protons by xenon nuclei[5]. Thus it was first necessary to select a sample of Λ^0 decays as observed in the Xenon Bubble Chamber. Second, it was necessary to scan each decay proton for scatterings by xenon nuclei. Third, it was necessary to correlate the proton scattering plane with the proton direction in the Λ^0 rest frame as described in Chapter V. The measurement of the sign and magnitude of α was then accomplished within the limits of the statistical uncertainties and biases of this experiment.

II. EXPERIMENTAL EQUIPMENT

2.1 The Xenon Bubble Chamber

The particle detection apparatus used in this experiment was a Xenon Bubble Chamber. The properties of xenon, making it valuable as a bubble chamber liquid, have been discussed elsewhere[6]. The principal attribute of xenon in a polarization scattering experiment is its high density -2.17 gm/cm^3 at -21.5°C. By using a liquid with such a high density one can expect a short nuclear-scattering mean-free-path. Thus, in contrast to a light liquid chamber, a larger proportion of the protons from the decaying Λ^0 hyperons undergo scattering from nuclei before they leave the chamber.

The sensitive volume of the Xenon Bubble Chamber was approximately 21 liters, with 18.5 liters illuminated for photographing the tracks. The chamber contained .5% ethylene by weight, which was found necessary for the proper operation of xenon as a bubble chamber fluid[7]. Figure 1 is a schematic cross section of the Xenon Chamber, as it appeared in the summer of 1958, showing the necessary details. Note that the sensitive volume was cylindrical, 12 inches in diameter and 10 inches long. Dark field photography was accomplished by using a beam of parallel light passing through the chamber. The camera lenses were positioned outside the light beam at an average stereo angle of 35°. A General Electric FT-230 flash tube positioned at the focus of a 12 inch diameter condensing lens provided the illumination with a light pulse of 100



Michigan Xenon Bubble Chamber Summer 1958

Side view Cross section

Figure 1. Bubble Chamber Cross Section

microseconds long. Both the camera and the flash tube looked at the chamber via front surfaced mirrors.

The camera lenses were a matched pair of Schneider Super Angulons with a focal length of 65 millimeters stopped down to f/45 to obtain the necessary depth of field. The film was 70 millimeter Kodak Linagraph Panchromatic. Vacuum film backs were used to obtain a flat and reproducible film plane. The camera was bolted firmly to the bubble chamber to avoid any shift of the optical axes with respect to the chamber.

To obtain a reference system with respect to the bubble chamber, special grid marks were placed on the inside of the chamber windows. These consisted of .0005 inch diameter to .0015 inch diameter glass beads suspended in an epoxy resin. Their index of refraction was 1.92, hence they scattered the light effectively at large angles, even though the index of refraction of the resin was 1.51. The suspension was applied to the windows with a #27 hypodermic syringe needle mounted on the traveling arm of a precision shaper. The resin was then cured at 60°C. With this method grid marks .010 inches wide were deposited 2.000 ± .002 cm. apart.

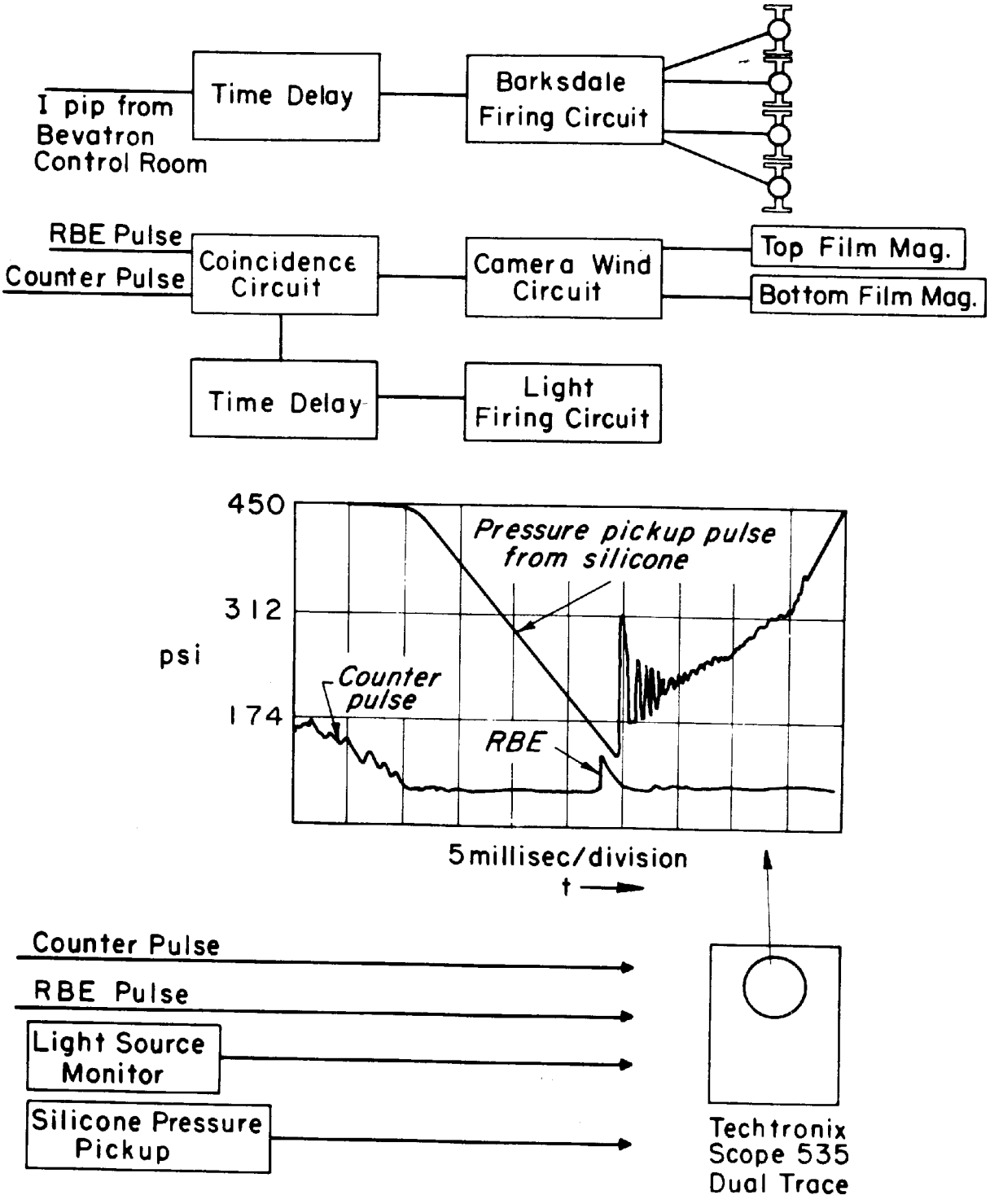
The expansion system of the chamber consisted of an air-driven aluminum piston moving a hydraulic fluid supporting a rubber diaphragm which separated it from the liquid xenon. Initially the chamber was filled with xenon by distillation from the reservoir tanks until only 3.5% of the chamber volume contained vapor (the remainder being filled with liquid xenon at -21.5°C.). At this point the diaphragm rested on the perforated steel plate and the piston was at its extreme lower position. Hydraulic fluid was then introduced until the vapor volume had

been reduced to 2.5% of the chamber volume. Compressed air at 430 p.s.i.g. then entered through four Barksdale valves, forcing the piston up and completely compressing the remaining vapor since the vapor pressure of xenon is 370 p.s.i. at -21.5°C. Upon initiation of expansion, the air under the piston was opened to the exhaust system by the Barksdale valves. The over pressure on the liquid xenon forced the piston down to its lower bumper, thus increasing the volume of the liquid by 2.5% and bringing it into the necessary superheated and sensitive state. After the expansion the xenon was recompressed by opening the Barksdale valves to the compressed air supply and thereby raising the piston.

The refrigeration of the chamber was accomplished by circulating a brine through cooling plates attached to the exterior of the chamber. The brine, consisting of 50% water and 50% ethylene glycol by volume, was cooled by a refrigerator. Regulation of the temperature to .1°C. was accomplished by a thermostat controlling a 9 kilowatt heater in the brine line.

The Xenon Bubble Chamber was operated in a concrete block house in the experimental area of the Bevatron at the Lawrence Radiation Laboratory, Berkeley, California. The π^- meson beam came from a target in the west straight section and was used simultaneously by the bubble chamber and a counter group[8]. For the first 60,000 pictures the average beam kinetic energy was 1.0 Gev, while the pictures from 60,000 to 160,000 had an average beam kinetic energy of 1.1 Gev, except for pictures 104,037 to 106,606 for which the energy was reduced to .8 Gev.

Figure 2 is a schematic of the bubble chamber electronic system and shows how the beam was shared. The majority of the circulating



Schematic of Bubble Chamber Electronics
Summer 1958

Figure 2. Schematic of Bubble Chamber Electronics

protons in the Bevatron were dribbled into the target in the straight section over a period of 50 milliseconds producing approximately 10^5 pions at the counter group's hydrogen target in this time. The minute fraction of protons remaining was then steered away from the target for 20 to 25 milliseconds and then slammed into it again in less than 10 microseconds by the rapid beam ejector (RBE) to produce 8 to 10 pions at the bubble chamber. The lower oscilloscope trace in figure 2 shows a typical pattern as seen by our beam monitor. The 20 to 25 milliseconds with no beam allowed the chamber to expand with no background from the counter pulse.

The sequence of operation of the chamber with the Bevatron was as follows:

1) A timing pulse (I pip) was received from the control room initiating a delayed pulse that fired the Barksdale valves. The delay was set so that the RBE pulse fell near the bottom of the expansion cycle (upper oscilliscope trace in Figure 2).

2) The RBE pulse from the control room initiated a delayed signal which fired the flashtube approximately 2 milliseconds after the pions arrived and triggered the film-winding mechanism. The flash tube firing was timed from the RBE as there usually was jitter and drift in the timing between the I pip and the RBE.

A scintillation counter monitored the beam entering the chamber. A fast scaler, gated only during the RBE pulse, counted the number of pions per pulse seen in the bubble chamber. A scaler, in parallel with one above, was installed in the Bevatron control room to allow the Bevatron

operator to monitor the beam.

2.2 The Scanning Equipment

Once the film had been developed and divided into 400 picture rolls, the scanning was carried out at the University of Michigan's Randall Laboratory. The scanning machines projected the film image onto a scanning table from above at about life size. The projected images from the two stereo pictures could be superimposed by means of levers attached to the projectors.

At the time of the film exposure, a small area on each frame was exposed to light. Upon development these spots were used to control an automatic film stopping mechanism on the scanning machines. When the scanner had finished scanning one frame and was ready for the next, the film-drive motors were started, advancing the film until the black spot on the next frame was seen by a photodiode. The corresponding pictures were usually aligned well enough by the automatic stop so that no further film motion was necessary. This device greatly increased the scanning speed.

2.3 The Measuring Equipment

Pictures to be measured were projected onto a green, translucent screen. By moving the stages to which the film was attached, the measurer positioned the particular point to be measured on a crosshair fixed to the green screen. In this way non-uniformities of the projection optics did not affect the accuracy of the measurements. Two magnifications provided both an overall view of the picture and a detailed view of a smaller portion of it. The lower magnification gave an image 1.75 times actual size, while the higher magnification gave one 4.25 times

the actual bubble chamber size. All measuring was performed at the higher magnification.

Two measuring engines were used in the data reduction. The film stages in one measuring engine were driven by precision screws that were accurate to one micron per centimeter. Wang encoders were attached to the screws and gave the linear positions of the stages in binary numbers. This information, converted electronically to decimal form, was automatically punched onto IBM cards. To insure correct conversion from binary to decimal, two independent conversions for each of the two axes of motion were always performed and compared electronically before punching was allowed.

The second measuring engine used a Ferranti Moiré fringe counter to determine the linear positions of the film stage to .0001 inch In this system reversible scalers counted the number of fringes passing a photodiode--aiding or subtracting counts depending upon the direction of travel of the stage.

One of these fringe detectors and scalers was used for each of two axes of motion of the stage. The scalers employed dekatron tubes automatically giving a scale of ten. Checks for spurious addition or subtraction of counts were easily accomplished by observing the coordinates of the center grid mark on each picture before and after each event was measured. The coordinates as indicated by readings on the scalers were punched on IBM cards.

III. DATA REDUCTION

3.1 Scanning and Measurement

The reactions of interest in all the studies performed in this meson exposure involved V^0 particles. That is, either a K^0 or a Λ^0 was present in all the pictures of interest. Thus the pictures were scanned for V^0 particles, their origin, their associated reactions and their associated strange particles. Any V^0 particle found was sketched on a scanning sheet and recorded on a scanning tally list. The sketch included the π^- interactions which could be the production points of the V^0 particle; the bubble density of the tracks; notes indicating whether the legs of the V^0 stopped by ionization, interacted, or went out of the chamber; and the number of incoming beam tracks.

The reactions of π^- mesons in the Xenon Bubble Chamber which resulted in the production of Λ^0 particles were classified in the following way:

1) $\pi^- + Xe \longrightarrow \Lambda^0 + K^0 + \text{NUCLEONS}$

2) $\pi^- + Xe \longrightarrow \Sigma^0 + K^0 + \text{NUCLEONS}$

$\Sigma^0 \hookrightarrow \Lambda^0 + \gamma$

3) $\pi^- + Xe \longrightarrow \Lambda^0 + K^+ + \text{NUCLEONS}$

4) $\pi^- + Xe \longrightarrow \Sigma^\circ + K^+ + \text{NUCLEONS}$

$\hookrightarrow \Lambda^\circ + \gamma$

Λ°'s from the reactions 1) and 2) were combined in all studies of π^- interactions resulting in the production of 2 V° particles. Λ°'s from the reactions 3) and 4) were combined in all studies of π^- interaction producing one V° particle and one charged strange particle. This division was prompted by the supposition that the Λ° detected in reactions 3) and 4) were produced by Σ^- interactions with protons inside the target nucleus. Thus there was no guarantee that the polarization of the Λ° so produced would be the same as the polarization of Λ° produced via reactions 1) and 2). A difference in polarization was in fact found (See Chapter VI).

The staff and the graduate students of the bubble chamber project scanned the first 86,000 pictures while professional scanners scanned the frames from 86,000 to 160,000. Many of the film rolls were scanned by several persons. By comparing the results, it was shown that very few events were missed. Note, however, that the scanning efficiency does not affect the value of α as found by this experiment.

The measuring method employed was that of corresponding points. That is, the same point or bubble was measured in both of the stereo views. The large stereo angle (35°) allowed much better measuring accuracy in depth than the ordinary bubble chamber optical systems. The distance between points in the plane of the chamber windows could be determined to within $\pm$ .015 cm, while the distance between points on an

axis perpendicular to this plane could be determined to within ±.03 cm.

On each view the center grid mark on the front window was measured at the beginning of each measurement to provide a reference point in the chamber. This grid mark was the origin of a coordinate system in which all events were calculated. At the end of each measurement two other grid marks were measured on each view to check for rotations of the film. Then the center grid mark was remeasured to check the encoders or fringe counters.

All V^o events were measured in the frames up to 105,000. From 105,000 to 160,000 only V^o particles from beam interactions were measured. Only obvious scanning errors were disregarded. Examples of these would be: neutron stars with three charged prongs one of which could only be seen under high magnification, scattered beam tracks simulating V^o's, or interactions V^o's. The space coordinates of each point measured were calculated from the data on the IBM cards by an IBM 650 computer during the first half of the experiment and by an IBM 704 during the second half of the experiment. From the space coordinates and the coded remarks about each point, the computer calculated the following:

1) Ranges of V^o legs
2) Length of flight of V^o
3) Direction cosiness of pion beam track
4) Direction cosines of V^o path
5) Direction cosines of V^o legs
6) Angle between the plane of the V^o legs and the V^o path----the coplanarity angle
7) Total opening angle between legs of V^o

8) Angle between each leg and the V^o path

9) Angle between the V^o path and the beam direction

10) Check quantities to check the operation of the measuring engine and the computer.

The above were printed in a convenient form for each event measured.

3.2 Analysis of Events

The range-energy relations for the various particles were calculated by Professor George Trilling using the Bethe-Bloch formula and parameters as given by Sternheimer[9] and Walske[10]. These calculations were checked by measuring the range of the pions from five $K_{\pi 2}$ decays at rest in which the π^+ came to rest in the chamber. Good agreement was found between the predicted and the measured ranges.

Using the range-energy relations along with the kinematical relations for the decay of Λ^o particles, the following graphs were drawn:

Graph 1) Range of proton (Rp) vs. Range of pion (R_π) for various total opening angles between the Λ^o decay products (θ_Λ);

Graph 2) Range of proton (Rp) vs. total opening angle between the Λ^o decay products (θ_Λ), for various angles between the proton and the Λ^o path (θ_p);

Graph 3) Range of decay pion (R_π) vs. total opening angle (θ_Λ), for various angles between the pion and the Λ^o path (θ_π);

Graph 4) Angle between the pion and the Λ^o path (θ_π) vs. the angle between the proton and the Λ^o path (θ_p), for various Λ^o momenta and angles between the pro-

ton and the Λ^o path in the Λ^o rest frame (θ_p^*).

Using the range-energy relations and the kinemetical relations for the decay of K^o mesons, the following graphs were drawn:

Graph 5) Range of decay pion (R_π) vs. the total opening angle between the K^o decay products (θ_K), for various angles between the decay pion and the K^o path ($\theta_{\pi 1,2}$);

Graph 6) Angle between one decay pion and the K^o path ($\theta_{\pi 1}$) vs. the angle between the other decay pion and the K^o path ($\theta_{\pi 2}$), for various K^o momenta and angles between one of the pions and the K^o path in the rest frame of the K^o meson (θ_π^*).

Three classes of events were defined for the purpose of analysis:

Class 1) Events in which both decay products (i.e., legs) of the V^o stopped by ionization in the chamber;

Class 2) Events in which one leg stopped by ionization, and the other leg left the chamber or interacted before leaving the chamber;

Class 3) Events in which both legs left the chamber, or one leg interacted and one left the chamber, or both legs interacted before leaving the chamber.

Each of these classes was analysed in a slightly different manner. The class in which both legs stopped by ionization contained more information than was necessary to determine if an event was a Λ^o. For instance, the range of the pion and the proton uniquely determined the total opening angle, θ_Λ, without the necessity of knowing the proton - Λ^o angle,

θ_p , or the pion - Λ^o angle, θ_π.

Analysis of events in all three classes began with a check of the coplanarity angle for all beam interactions measured. If the V^o path length was greater than .5 cm and the coplanarity less than seven degrees, the event was called coplanar to that interaction and may have come from it. If the V^o path length was greater than .5 cm and the coplanarity angle greater than seven degrees, the event was considered not coplanar to that particular interaction when there we no obvious measuring errors. If the V^o path length was less than .5 cm, the angular errors in θ_p(or θ_{π_1}) and θ_π(or $\theta_{\pi 2}$) were large and the final decision had to rest on subsidiary information such as the bubble density of the decay products, the comparison of the calculated θ_Λ with the measured quantity if possible, and the evidence for an associated strange particle from that particular origin. The choice of a limit of seven degrees on the coplanarity angle was made through an examination of the double V^o events (See Figure 3). As a further check the sum of the angles θ_p(or θ_{π_1}) and θ_π (or $\theta_{\pi 2}$) had to equal the total measured opening angle θ_Λ(or θ_K) to within two degrees. Further analysis employed the graphs mentioned above.

If the event was in class 1) then the total opening angle, θ_Λ, was determined from graph 1). The quantity, δ, was defined by

$$\delta = \frac{\theta_\Lambda(\text{FROM GRAPH 1}) - \theta_\Lambda(\text{MEASURED})}{\theta_\Lambda(\text{MEASURED})}$$

If $|\delta| \leq .15$, the V^o was considered to be real, independent of the coplanarity angle. The limiting value of δ was chosen by inspection of the distribution of δ observed for all Λ^o's both legs of which stopped

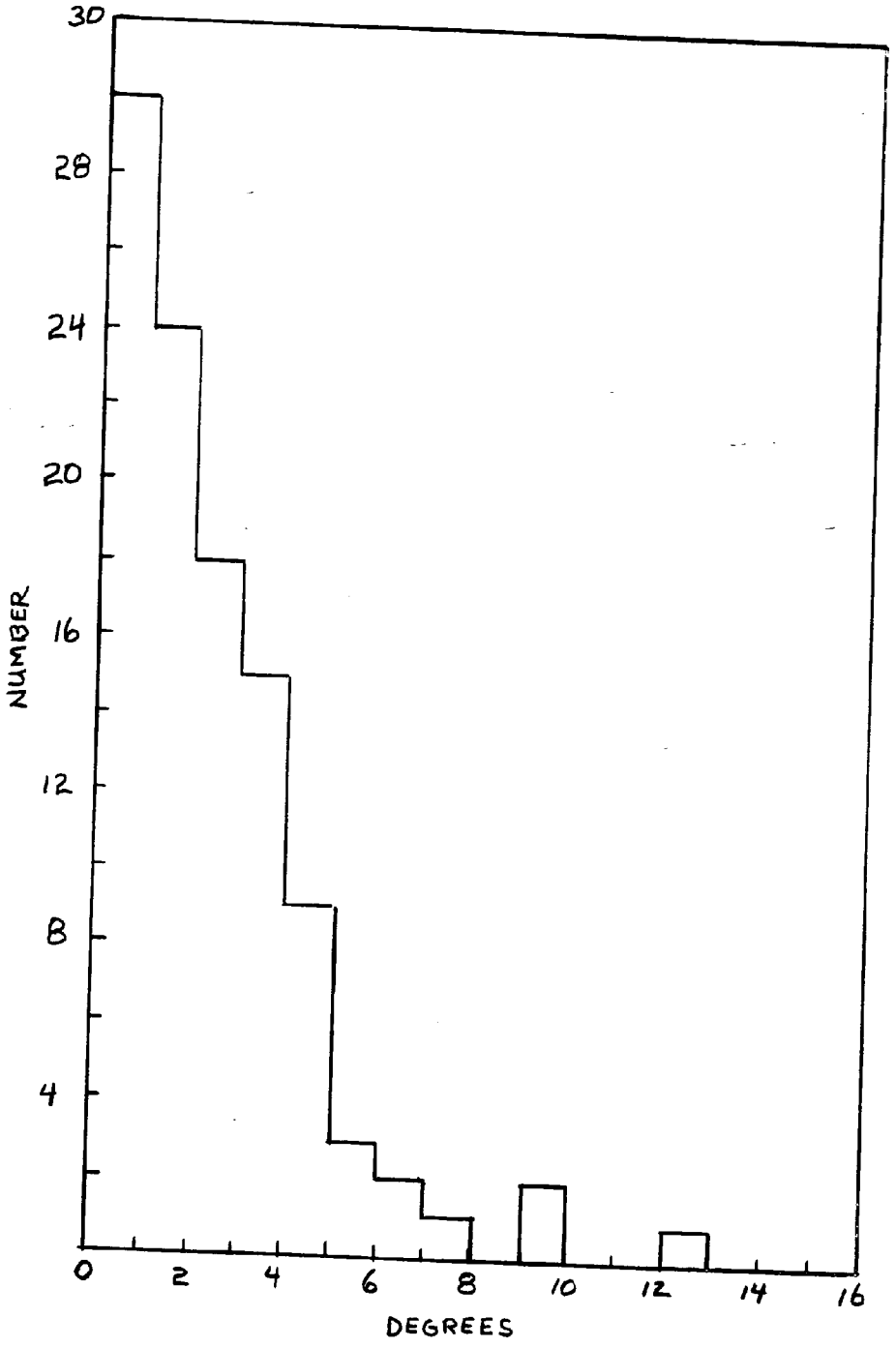


Figure 3. Distribution of Coplanarity Angle (105 Λ^{o}-K^{o} Events).

by ionization, (Figure 4). It was further required that these Λ^0's be associated with a coplanar, unambiguous K^0 decay. The criteria, $|\delta| \leq .15$, alone eliminated 90% of the background of secondary stars, but only 9% of the Λ^0 sample.

No K^0 events exist in Class 1), as it is kinematically impossible for a K^0 to decay in such a manner that both of its decay products would come to rest in the volume of the chamber. If δ was greater than $-.15$, one leg was assumed to have interacted and the event placed in Class 2). If δ was less than $-.15$, the proton-Λ^0 path angle, Θ_p, was read from Graph 2), using the opening angle determined from Graph 1). (The calculated opening angle was used instead of the measured value as the ranges of the legs provided a more accurate determination of Θ_Λ.) Similarly, the pion - Λ^0 path angle, Θ_π, was read from Graph 3). The calculated angular errors from multiple scattering were added to the calculated angular errors from measuring inaccuracies providing a total expected angular error for each event. If the event was coplanar and Θ_p and Θ_π agreed with the measured values to within the expected angular error, the event was called <u>real</u> to the beam interaction specified.** The momentum and Θ^*_Λ were then determined from Graph 4). If the angles did not agree, the event was called <u>not real</u> with respect to the beam interaction specified.

Events in Class 2) were handled in a similar way to those in Class 1), with regard to their coplanarity and measured angles. The visible

**The correctness of the calculated angular errors was confirmed by comparing the measured and calculated angles for Λ^0's having both decay products stopping in the chamber and accompanied by a K^0 decay.

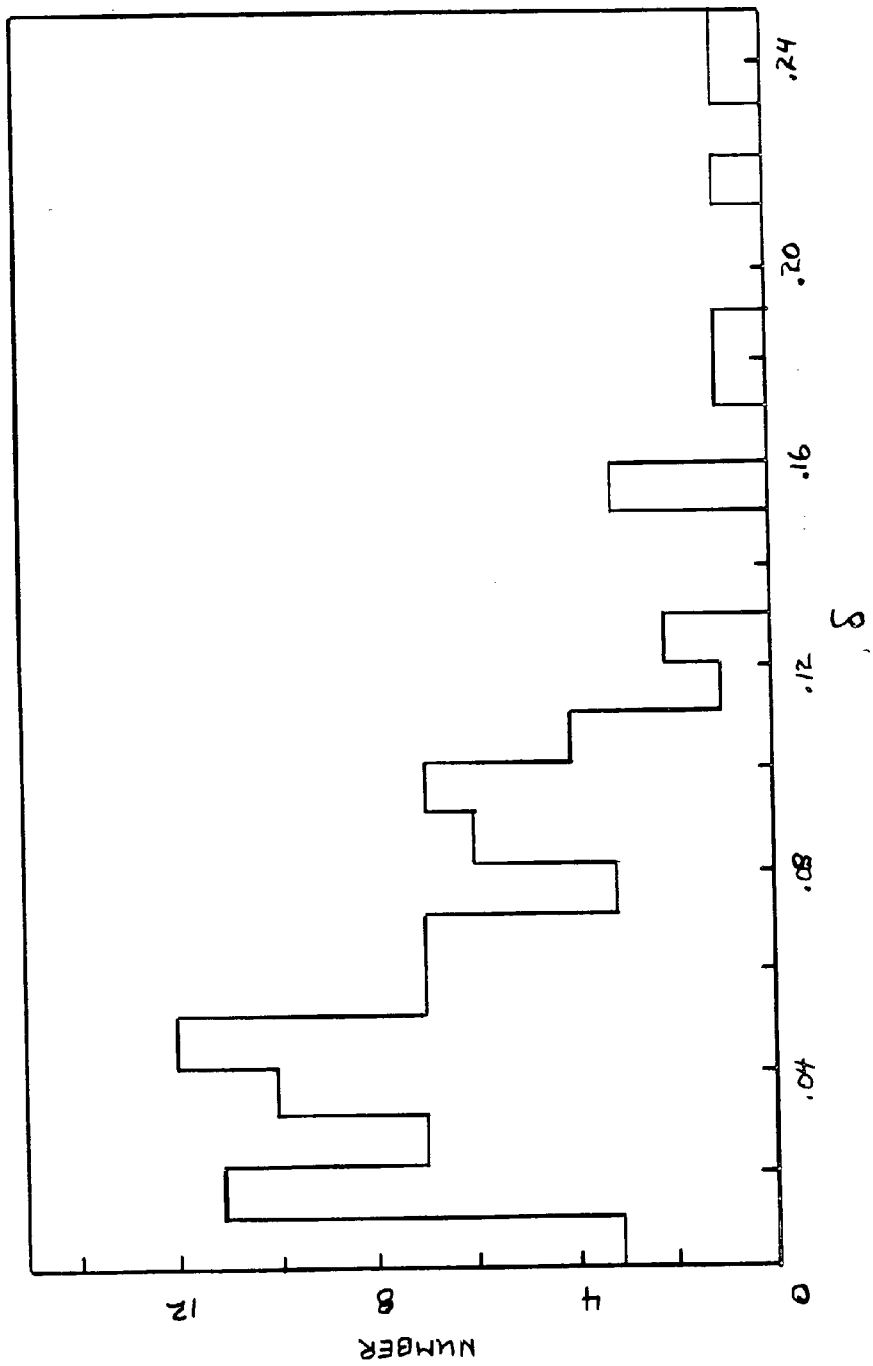


Figure 4. Distribution of δ (88 Events).

path length of the decay products enabled one to calculate a maximum total opening angle if the V^0 was a Λ^0, since an increase in length of either leg could only decrease $\Theta_{\pi p}$. The leg with the smaller angle to the path was considered to be the proton and the other, the pion. If the calculated opening angle was smaller than the measured opening angle, the event could not be a Λ^0. Events such as these were analysed as K^0 meson decays. If the calculated opening angle was larger than the measured opening angle, the event could be either a Λ^0 or K^0 decay. Since the range of only one of the decay products was known, the measured opening angle had to be used to calculate the expected value of the angle between the stopping particle and the V^0 path. Again using the leg with the smallest angle to the Λ^0 path as the proton, the calculated leg-to-Λ^0-path angle from Graph 2) or Graph 3) was compared to the measured value, and the range of the non-stopping particle was determined from Graph 2) or Graph 3). The momentum was found from Graph 4) and the angles calculated. If these angles and ranges were in agreement with the measured values, (taking into account the measuring inaccuracies and multiple scattering of the tracks), the event was considered consistent with being a Λ^0 decay. If they were not in agreement, the event was considered to be a possible K^0 decay.

All events whether consistent with being a Λ^0 decay or not, were next analysed as K^0 decays. Using the range of the stopping leg and the measured opening angle, $\Theta_{\pi\pi}$ was calculated from Graph 5) and $\Theta_{\pi z}$ deduced. From these angles the K^0 momentum was determined from Graph 6). The range of the non-stopping leg was also found from Graph 5). If the

calculated ranges and angles were in agreement with the measured values, the event was called a K^o decay. Often events were kinematically consistent with being either a Λ^o decay or a K^o decay. In these cases the first differentiating factor was whether another strange particle from the same beam interaction was present, the identity of which could be determined unambiguously. If so, the case rested. If not, the appearance of the event was checked in rescanning. When a π-μ-e decay was visible at the end of one of the legs, the event was classified as a K^o decay, as a π^- meson is absorbed 99.9% of the time[11]. Bubble density and multiple scattering were used as further checks. In this manner all but a fraction of a percent of the events were identified unambiguously. The unidentifiable events were not used in this study.

The events falling into Class 3) were mainly K^o decays. As no angles could be calculated to check consistency with a specific origin, the coplanarity angle assumed great importance. A check of consistency with Λ^o decay was possible by using the visible ranges as was done with Class 2) events. The momenta were determined using the measured angles. A V^o momentum greater than 900 MeV/c cast doubt on the identification of the event as a K^o; and a momentum greater than 1300 MeV/c cast doubt as to the reality of the event as a K^o. An associated and uniquely identifiable strange particle was considered as positive identification. The calculated ranges of the decay products were checked against bubble density and multiple scattering and the consistency demanded. In this manner all but a few events were unambiguously identified. Those events, the identity of which could not be ascertained, were not included in the sample for this study.

3.3 Detection of Proton Nuclear Scatterings

After a sample of bonafide Λ^o decays had been selected, it was necessary to detect the nuclear scatterings of the protons arising from these decays. Each event was rescanned for scatterings at least once. The author performed all the rescanning for scatterings and the measurement of all the scatterings found.

The event to be scanned for scatterings was placed on the measuring engine and projected onto the green, translucent screen. The proton track was scanned through a glass rod 1.2 cm in diameter and 10 cm long. The rod acted as a cylindrical lens, magnifying perpendicular to its axis but not parallel to it. Thus, when the axis of the rod was placed parallel and over a proton track, any deviation of the bubble from a straight line was visible. A scattering as small as two degrees was easily discernible; the point of scattering, easily discovered. The rod exaggerated the gentle curvature of multiple coulomb scattering in such a way that single scatterings could be separated from multiple scatterings within a length of track .3 cm long.

The calculated root-mean-square, multiple coulomb scattering angle[12], Θ_{RMS}, over a distance of .3 cm is shown in Figure 5 as a function of proton energy. At a given proton energy, Θ_{RMS} was smaller than any useful scattering angle (See Figure 7), and was in most cases a small fraction of the total scattering angle. Thus, the contamination of the sample by apparent nuclear-scattering events simulated by multiple scattering was considered to be negligible.

As a further check on the purity of the scatterings, the proton-silver elastic differential scattering cross sections were used to

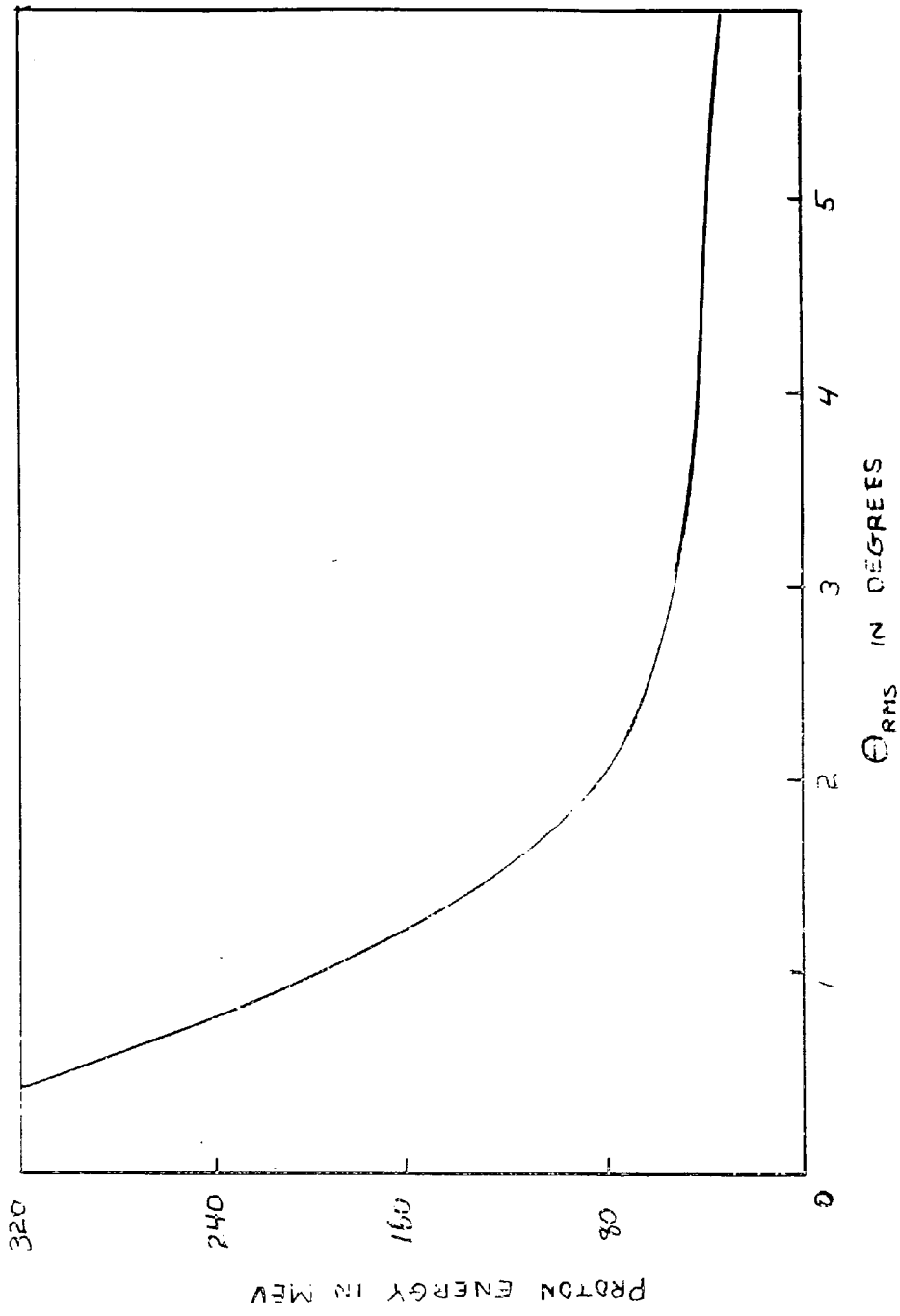


Figure 5. Θ_{RMS} Over .3cm as a Function of Proton Energy.

calculate the number of events expected. The proton-silver cross sections at 17 MeV[13], 96 MeV[14], 138 MeV[15], and 340 MeV[16] corrected by an $A^{2/3}$ factor were used, since there were no proton-xenon scattering cross sections available over this energy range. The 96, 138, and 340 MeV cross sections were integrated from 5° to 20°, while the 17 MeV cross section was integrated from 15° to 45°. In the frames from 0 to 100,000, 62 ± 3 scatterings were expected in these angular and energy intervals, and 59 scatterings were found. Thus, it was assumed that contamination of the sample by multiple coulomb scattering was small and that the detection efficiency was high.

It was also necessary to check the accuracy to which a scattering could be measured. 28 scatterings were remeasured and the angles checked against the first measurement. From this study it was concluded that the scattering angle could be measured to within $\pm 1.5^{\circ}$. The error introduced in this manner was negligible when compared to the overall statistical uncertainty in the measurement.

IV. DETERMINATION OF PROTON POLARIZATIONS

4.1 Polarization Scattering

The asymmetric scattering of transverse polarized protons from nuclei is well known[5]. The effect is one of spin-orbit interaction between the proton and the whole nucleus. The experimentally observed distribution of scattered protons at a given energy, E, can be described by

$$F(V_t, S, \phi) = \frac{1}{2\pi}\left(1 + V_t\, S(\theta, E) \cos\phi\right)$$

where V_t is the magnitude of the transverse polarization of the incident proton, θ is the angle through which the proton scattered, ϕ is the angle between the normal to the scattering plane and the proton polarization direction, and $S(\theta,E)$ is the analysing strength which measures the magnitude of the effect at a given angle, θ . The normal to the scattering plane is defined[17] as

$$\hat{n} = \frac{\hat{k}_i \times \hat{k}_f}{|\hat{k}_i \times \hat{k}_f|}$$

where $\hat{k}_i$ is direction of the proton before the scattering, and $\hat{k}_f$ is the direction of the proton after the scattering. J. Marshall and L. Marshall[18] have shown further that when the proton spin is up, $S(\theta,E)$ is positive, i.e., the proton scatters preferential to the left.

Although $S(\Theta,E)$ has been measured for many materials, at many energies, E, and angles, Θ, it has never been measured for xenon as far as the author could determine.

4.2 Analysing Strength of Xenon

To determine the analysing strength of xenon, $S(\Theta,E)$, as a function of incident proton energy, it was necessary to determine if the dependence could be extrapolated from data on elements which had been studied extensively. To check the feasibility of extrapolating the known data into the unknown region, the dependence of $S(\Theta,E)$ on the atomic number, A; the nuclear charge, Z ; and the spin of the ground state of the struck nucleus was investigated.

Alphonce, Johansson, and Tibell[19] have shown that there is no essential difference in $S(\Theta,E)$ for iron, copper, or nickel even though the ground state of copper has a spin of $\frac{3}{2}$ while iron and nickel both have zero spin ground states. Dickson, Rose, and Salter[17] have shown that there is no essential difference in $S(\Theta,E)$ for cadmium, silver, indium, and bismuth. Thus, as far as asymmetric proton scattering is concerned, all nuclei behaved as if they were spin zero nuclei. Kerman, McManus, and Thaler[20] have shown in their detailed analysis of scattering theory that this is exactly what should be expected.

The dependence of $S(\Theta,E)$ on Z has been discussed by Kerman, McManus, and Thaler[20]. Application of the expression which they derived showed variation in $S(\Theta,E)$ of less than one percent for Z from 12 to 82. Only in the scattering of protons at energies of less than 40 MeV and at angles of less than 10° did the effect reach one percent. These angular and energy regions, however, contained little if any information[21].

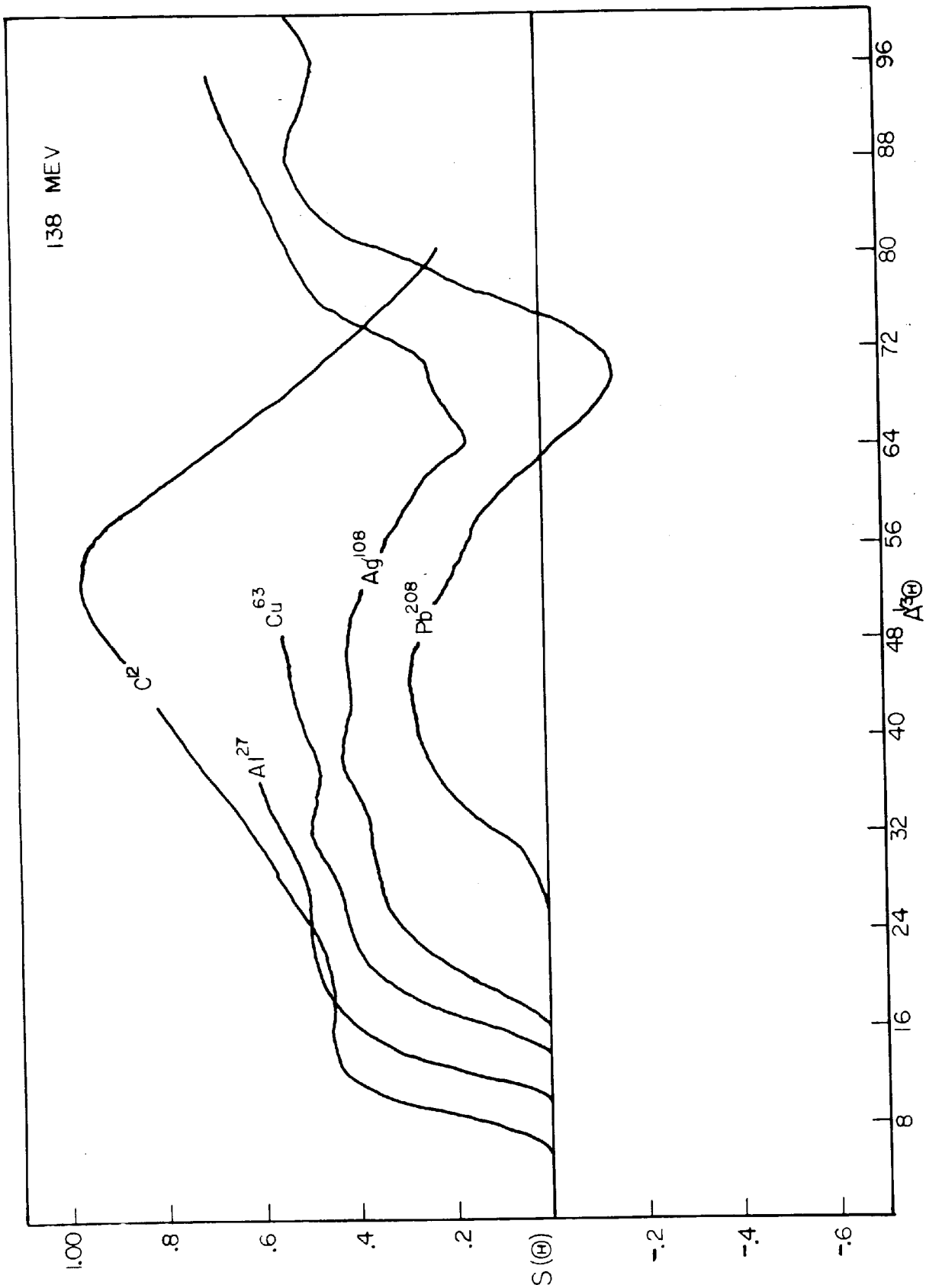


Figure 6. Analysing Strength for Several Elements at 138 MeV

When $S(\theta,E)$ at a given proton energy was plotted against $A^{\frac{1}{3}}\theta$, the curves for various elements assumed a similar shape as shown in Figure 6. The data was obtained from J. M. Dickson[15]. The quantity $A^{\frac{1}{3}}\theta$ is proportional to the momentum transferred from the proton to the stuck nucleus. The dependence of $S(\theta,E)$ on $A^{\frac{1}{3}}\theta$ is predicted by Kerman, McManus, and Thaler[20] and shown experimentally by Alphonce, Johansson, and Tibell[19]. This dependence allowed the interpolation between the existing data for silver and lead to obtain the necessary data for xenon.

The program for interpolating the data consisted of: 1)plotting $S(\theta,E)$ at each energy against $\theta A^{\frac{1}{3}}$ for all elements on which measurements had been made; 2) for each proton energy and value of $\theta A^{\frac{1}{3}}$ and $A^{\frac{1}{3}}$ plotting the value $S(\theta_i,E)$ for each element against $A^{\frac{1}{3}}$; 3)joining these points with a smooth curve and determining $S(\theta,E)$ for xenon by the intersection of the curve and the line $A^{\frac{1}{3}}=5.08$. At a proton energy of 138 MeV, data is available on C^{12}, Al^{127}, Cu^{63}, Ag^{108}, and Pb^{208} (15). At 99 MeV there exists data on C^{12} and Pb^{208} (15), while at 17 MeV[21] and 425 MeV[22] there is only data on Ag^{108}. From the constructed dependence of $S(\theta,E)$ for xenon on angle, θ, and proton energy, the contour maps shown in Figures 7 and 8 were drawn. Thus, in each scattering the angle, θ, and the energy of the incident proton determined the worth of that scattering as an analyser of the proton's spin direction.

Because of the limited data at 56 MeV and 99 MeV, the shaded area in Figure 7 represents a region of uncertainty in $S(\theta,E)$. At both of these energies the interpolation was between C^{12} and Pb^{208}. At both of these energies $S(\theta,E)$ for C^{12} was positive, while $S(\theta,E)$ for Pb^{208} was negative.

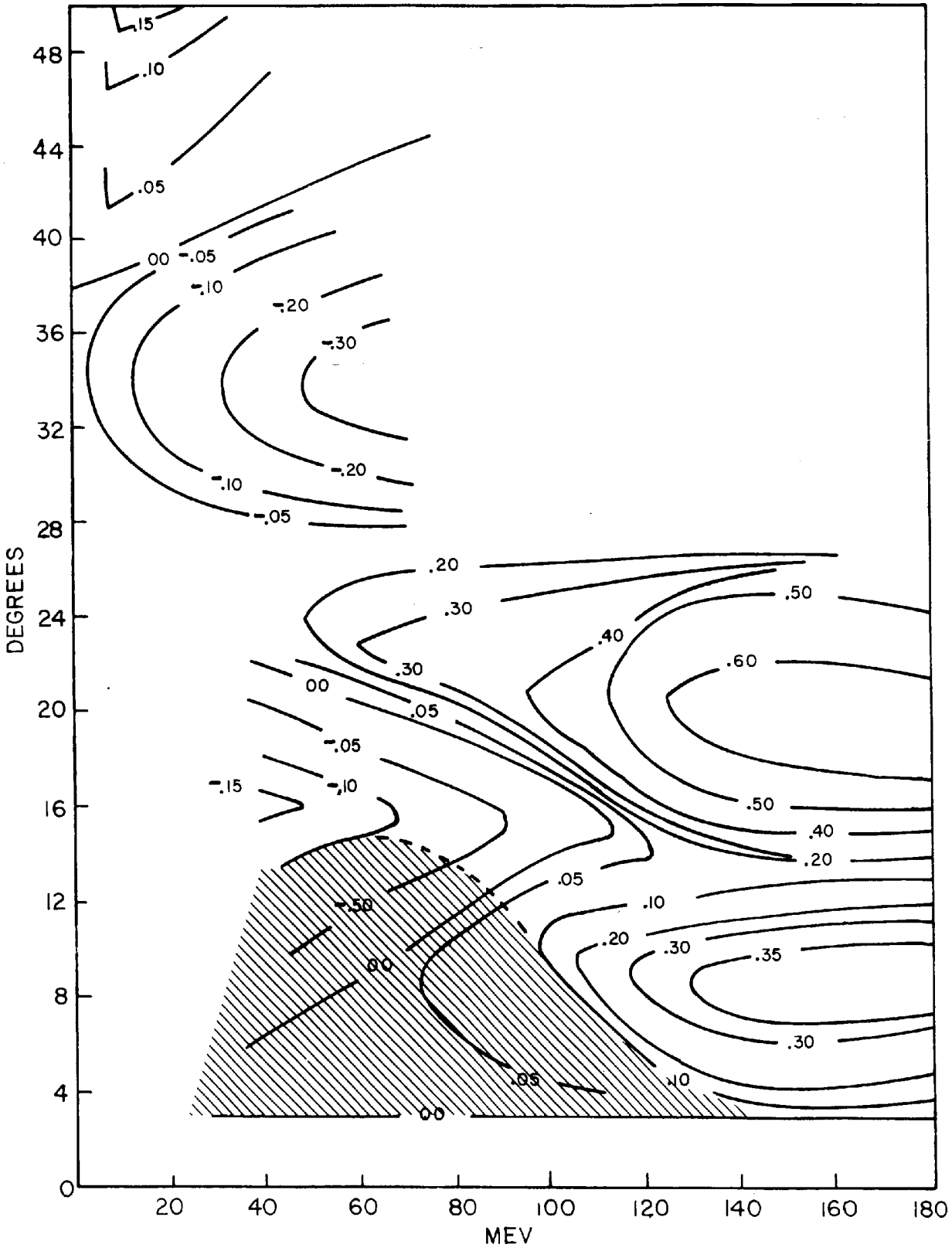


Figure 7. Analysing Strength for Xenon

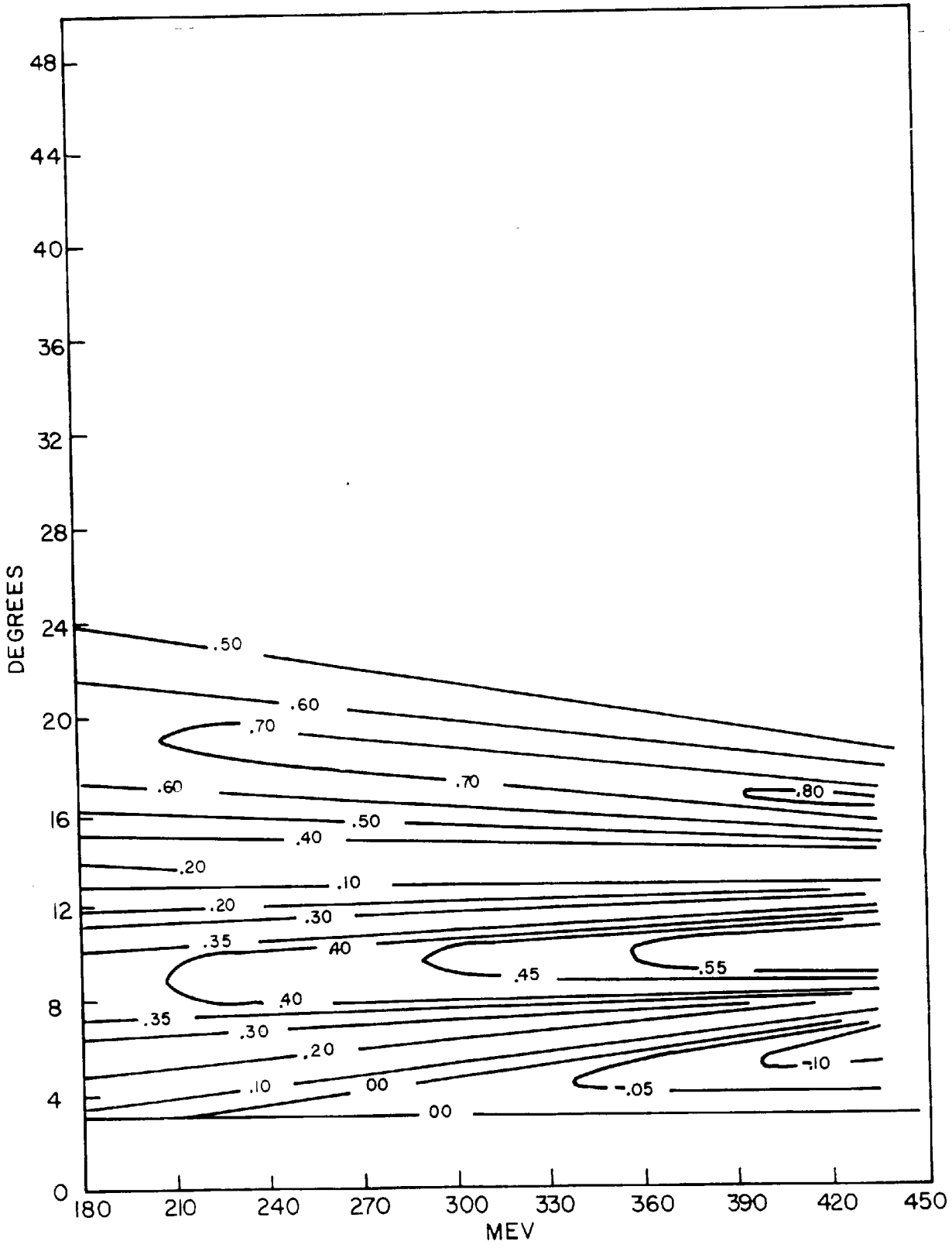


Figure 8. Analysing Strength for Xenon

Thus, the interpolation of the data to xenon might have been in error in both sign and magnitude.

4.3 Energy Loss on Scattering

The data [15,21,22] from which Figures 7 and 8 were constructed came from elastic scattering measurements. In practice this meant that the counter telescope detecting the scattered protons had an energy resolution of ±6 MeV or less, when set to the energy of the incident proton. The main concern was that no low-lying nuclear levels had been excited, i.e., levels lying 15 MeV or deeper. Hillman, Johansson, and Tyren[23] have shown that the $S(\theta,E)$ for 180 MeV protons scattered from carbon, with the excitation of 4.4 MeV and 9.6 MeV nuclear levels, is similar in sign and magnitude to the $S(\theta,E)$ obtained when no nuclear levels are excited, if θ is less than 35°. They have also shown that $S(\theta,E)$ is nearly zero at all angles, θ, when levels 15 MeV or deeper were excited.

Tyren and Maris[24] reported the proton-carbon cross sections for the excitation of the various nuclear levels. Happily, out to the first diffraction minimum all except the cross sections for exciting the 4.4 MeV and the 20 MeV levels are a factor of 100 or more less than the elastic cross section, i.e., the cross section when no nuclear levels are excited. Excitation of the 4.4 MeV level (which became important at scattering angles greater than 15°) causes no difficulties as is seen above. Excitation of the 20 MeV level is shown by Tyren and Maris[24] to be important in the region of first diffraction minimum, but $S(\theta,E)$ as determined from the elastic scattering data is small in this region. Thus, events near the first diffraction minimum have small weighting

factors.

Assuming that these general excitation and polarization phenomena are independent of the atomic number as predicted by Kermer, McManus, and Thaler[20], it was deemed necessary to eliminate from the sample all scatterings accompanied by an energy loss of approximately 20 MeV or greater.

To discover if it were possible to determine if there were energy loss at a given scattering, a study was made of the double V^0 events which had both Λ^0 decay products stopping by ionization inside the chamber. Further, the events chosen were required to have been an associated production with the coplanarity angles of both V^0's being less than seven degrees. The K^0 was required to have been identified as a strange particle independent of the Λ^0. The initial energy of the decay proton (from the Λ^0), E_m, was obtained from the proton range and the range-energy, E_c, was obtained from the total opening angle, Θ_Λ, and the angle between the proton and the Λ^0 path, Θ_p, with the use of analysing Graph 2). A quantity ΔE was defined by

$$\Delta E = E_M - E_c .$$

It can be seen from Figure 9 that the angular errors involved in determining E_c in a given event made it impossible to limit the acceptable events to those that had $|\Delta E|$ less than 20 MeV. The decision was made to eliminate all events with $|\Delta E|$ greater than 40 MeV. This criterion eliminated 20% of the scattering events that were inelastic by 20 MeV and 10% of the elastic scattering events. 17 events were thus removed from 90 scattering events in which the proton came to rest in the chamber. From the ratios of the elastic and inelastic cross sections[24] extrapolated

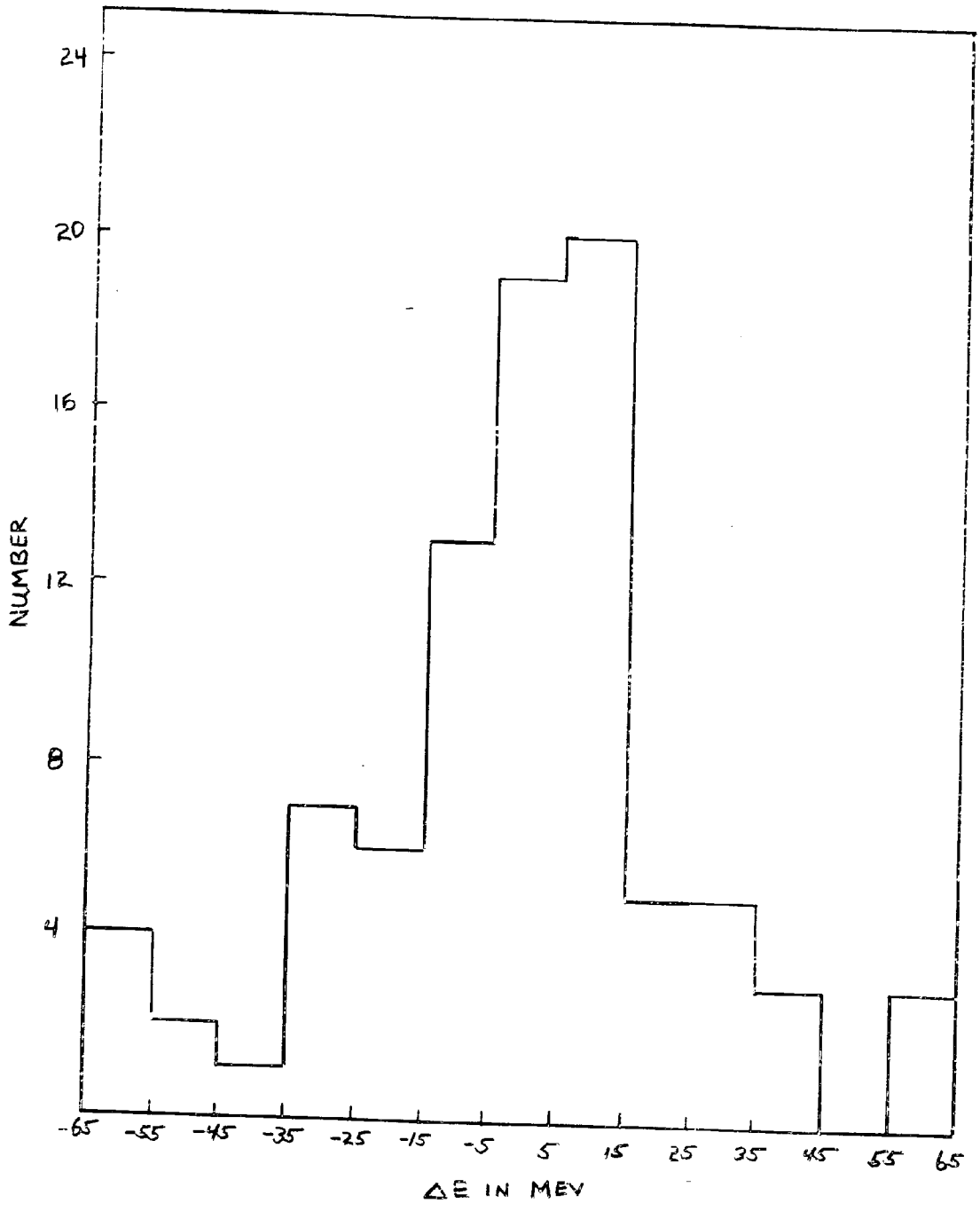


Figure 9. ΔE Distribution (88 Events).

to xenon, it was calculated that the 90 events concealed 20 scatterings that were inelastic by 20 MeV. As 20% if these were eliminated by the $|\Delta E|$ cutoff, there were yet 16 inelastic scatterings included in the "purified" sample.

40 scattering events remained in which the proton left the chamber. From the relative elastic and inelastic scattering cross sections, it was calculated that these 40 scatterings concealed eight scatterings that were inelastic by 20 MeV. As the proton did not stop in the chamber, there was no method by which the eight inelastic scatterings could have been gleaned from the sample.

The final sample used to measure the parameter, α, consisted of 113 scatterings, 28 of which had energy loss at the scattering of 20 MeV of greater. These 28 events affect the value of the result, α, and increase the errors in its determination.

V. DESCRIPTION OF α ANALYSIS TECHNIQUE

5.1 Description of Λ^0 Decay

For each Λ^0 decay a coordinate system was defined in the following way:

$$\hat{z} = \frac{\hat{k}_B \times \hat{k}_\Lambda}{|\hat{k}_B \times \hat{k}_\Lambda|}$$

$$\hat{y} = \hat{k}_\Lambda$$

$$\hat{x} = \hat{y} \times \hat{z}$$

where $\hat{k}_B$ is a unit vector in the direction of the π^- meson which produced the Λ^0 hyperon and $\hat{k}_\Lambda$ is a unit vector in the Λ^0 flight direction. A symbol with "$\wedge$" over it represents a unit vector, which a symbol with a "$\rightarrow$" over it represents any vector. (Note that the $\hat{z}$ direction is the axis of quantization for the Λ^0 spin.)

Figure 10 shows this coordinate system and some important angles associated with the decay. $\hat{k}_p$ represents the direction of the decay proton in the laboratory system and $\hat{k}_p^*$ represents the direction of the proton in the Λ^0 rest frame. Starred characters are quantities in the Λ^0 rest frame; unstarred characters are quantities in the laboratory system. χ^* and ν^* are, respectively, the polar, azimuthal angles locating $\hat{k}_p^*$ in x, y, z coordinate system. It was useful to observe that $\hat{k}_p$, $\hat{k}_p^*$,

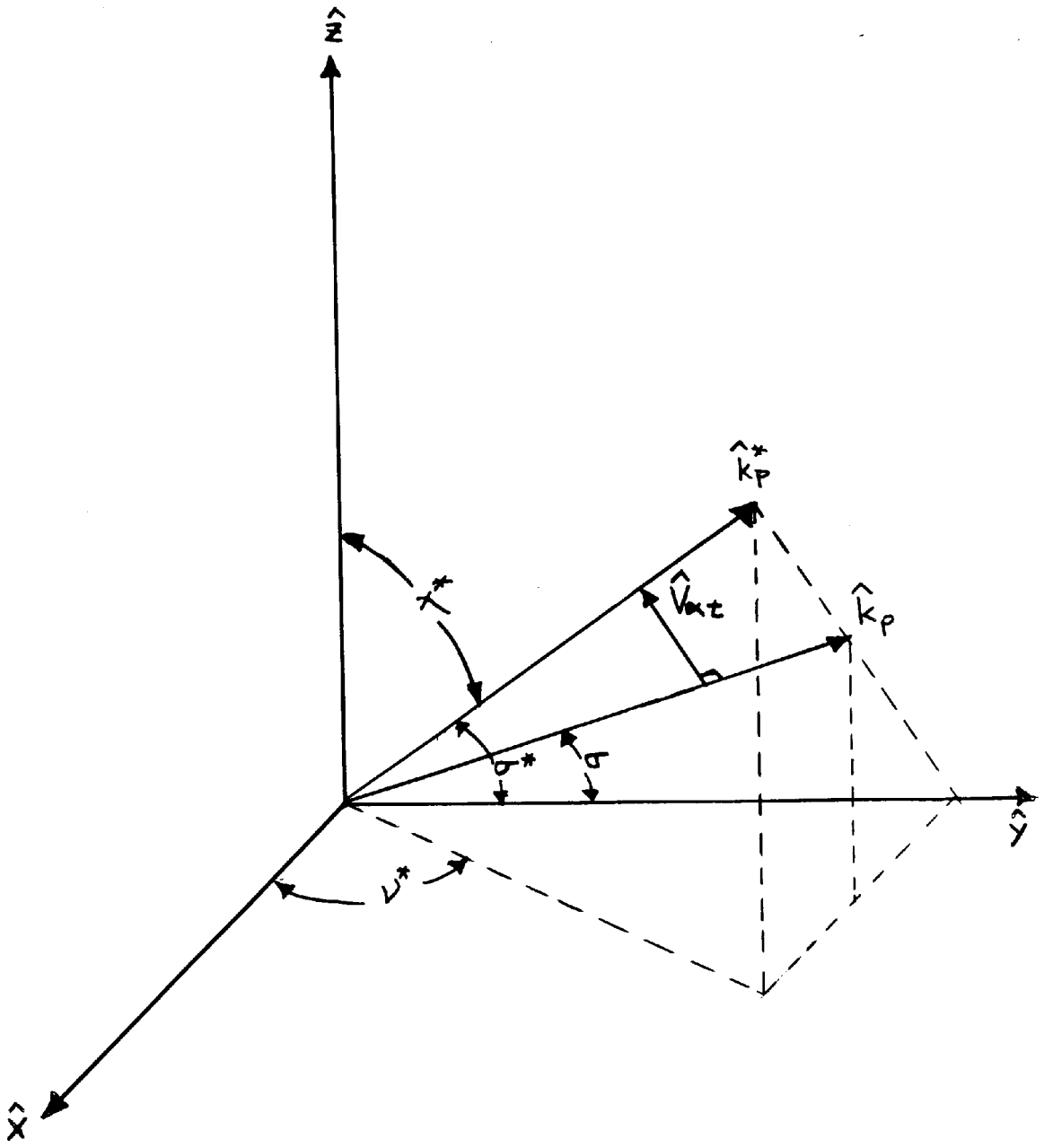


Figure 10. Coordinate System

and $\hat{y}$ all lie in the same plane - the decay plane.

The probability of observing a Λ^0 decay with the proton contained in the solid angle

$$d\Omega^* = \sin\chi^* \, d\chi^* \, d\nu^*$$

is

$$f(\chi^*, \nu^*) d\Omega^* = \frac{1}{4\pi}(1 - \alpha P \cos\chi^*) d\Omega^* .$$

Integrated over all ν^*, the probability becomes

$$f(\chi^*) \sin\chi^* d\chi^* = \frac{1}{2}(1 - \alpha P \cos\chi^*) \sin\chi^* d\chi^*$$

Here again the quantity P is the polarization of the hyperons, and α is expressed in terms of the complex amplitudes of the S and P waves in the decay, as shown in Appendix 8.1.

$$\alpha = \frac{2 \mathrm{Re}\, A^+ B}{A^2 + B^2} , \quad 0 \leq |\alpha| \leq 1 .$$

Two other quantities relating A and B are defined as shown in Appendix 8.1.

$$\beta = \frac{2 \mathrm{Im}\, A^+ B}{A^2 + B^2} , \quad 0 \leq |\beta| \leq 1$$

$$\gamma = \frac{A^2 - B^2}{A^2 + B^2} , \quad 0 \leq |\gamma| \leq 1 .$$

Using these quantities Lee and Yang[4] showed that the polarization of the decay proton from a Λ^0 hyperon is

$$\vec{V} = \frac{1}{1-\alpha P\cos\chi^*}\left[(-\alpha + P\cos\chi^*)\hat{k}_p^* + \beta P(\hat{k}_p^* \times \hat{z}) + \gamma P(\hat{k}_p^* \times \hat{z}) \times \hat{k}_p^*\right]$$

This formula is derived in the Appendix.

5.2 Realization of Transverse Polarization of the Proton

Inspection of the expression for $\vec{V}$, shown above, indicates that the component of the proton polarization involving the quantity α is longitudinal in the Λ^0 rest frame. The method of proton polarization analysis described in 4.1 is applicable only for transversely polarized protons. To obtain the necessary transverse polarization, the proton polarization was observed in the laboratory system. The realization of a transverse component of the polarization in this manner was possible because of the invariance of the proton spin under Lorentz transformations[25].

Hayakawa[26] has shown, however, that the spin was not exactly invariant under Lorentz transformations and that the longitudinal component of the spin in the new Lorentz frame is

$$V_L = \hat{k}_p \cdot \vec{V} - \beta_\Lambda \frac{k_p^*}{k_p}(\hat{y} \times \hat{k}_p^*)^2\left(1 - (1-\beta_\Lambda^2)^{-\frac{1}{2}}\right)$$

where V_L is the longitudinal component of the proton polarization in the laboratory system, β_Λ is the velocity of the Λ^0 in units of the

velocity of light, k_p^* and k_p are the magnitudes of $\vec{k}_p^*$ and $\vec{k}_p$, respectively, and $\vec{V}$ is the proton polarization in the Λ^0 rest frame as given in 5.1. An upper limit to the reduction of the transverse polarization due to this effect was calculated to be

$$\epsilon = \beta_\Lambda \frac{k_p^*}{k_p} (\hat{y} \times \hat{k}_p^*)^2 (1 - (1 - \beta_\Lambda^2)^{-1/2})$$

where ϵ is the reduction in magnitude. The quantity ϵ divided by the transverse component of the proton polarization was less than seven percent for $\beta_\Lambda < .8$ and $k_p > 300$ MeV/c. Thus, this effect was small compared with the other uncertainties of the measurements for every event in the sample.

In view of the above result, the simple, geometrical determination of the component of $\vec{V}$ perpendicular to the proton was used. Therefore, the transverse component of the proton polarization in the laboratory system could have been defined by

$$\vec{V}_t' = (\hat{k}_p \times \vec{V}) \times \hat{k}_p$$

However, this definition did not take into account one experimental fact - the proton underwent multiple coulomb scattering before scattering in a nuclear force field, with the result that their direction at decay was not exactly their direction immediately befcre the nuclear scattering occurred.

Hayakawa[26] derived an expression for the loss of polarization that a spin $\frac{1}{2}$ particle experiences in slowing from one energy to another. When this was applied to protons slowing down in xenon, the maximum loss of polarization was two percent, which occurred when 50 MeV protons

slowed to 17 MeV.* The loss of polarization was negligible compared to the uncertainties in determining $S(\Theta,E)$. Therefore, the assumption was made that the proton's polarization vector remained fixed in space even though the proton's direction was changed by multiple coulomb scattering. The transverse component of the proton polarization at the scattering was then defined by

$$\vec{V}_t = (\hat{k}_i \times \vec{V}) \times \hat{k}_i$$

where $\hat{k}_i$ is the proton direction immediately before scattering.

5.3 The Total Probability for Finding a Given Event Configuration

From a sample of Λ^0 which decayed via the mode

$$\Lambda^0 \longrightarrow p + \pi^-$$

the probability that the proton, as observed in the Λ^0 rest frame, is included in the angle between χ^* and $\chi^* + d\chi^*$ is shown in the Appendix to be

$$f(\chi^*) \sin\chi^* d\chi^* = \frac{1}{2}(1 - \alpha P \cos\chi^*) \sin\chi^* d\chi^*$$

For a particular scattering, the probability that the angle between the normal to the scattering plane and the proton's transverse polarization lies between the values ϕ and $\phi + d\phi$ was shown in Chapter 4 to be

$$F(\phi)\, d\phi = \frac{1}{2\pi}(1 + V_t\, S(\Theta,E) \cos\phi)\, d\phi .$$

V_t is the magnitude of the proton's transverse polarization. $\vec{V}_t \cdot S(\Theta,E)$ is the analysing strength for the scattering and was determined from the scattering angle, Θ, and the proton's energy, E, at the scattering. Cos ϕ is defined by

$$\cos\phi = \hat{n} \cdot \hat{V}_t$$

* No events with a proton energy of less than 17 MeV at the scattering were included in the sample.

where

$$\hat{n} = \frac{\hat{k}_i \times \hat{k}_f}{|\hat{k}_i \times \hat{k}_f|}$$

$F(\phi)d\phi$ could then be written

$$F(\phi)\,d\phi = \frac{1}{2\pi}\left(1 + V_t\, S(\theta,E)\,(\hat{n}\cdot\hat{V}_t)\right) d\phi .$$

Therefore, from a sample of Λ^0 decays whose protons scatter on xenon nuclei, the probability of observing a given event configuration within the angular region x^* to x^*+dx^* and ϕ to $\phi+d\phi$ is

$$P(x^*,\phi)\sin x^* dx^* d\phi = F(\phi)\,d\phi\, f(x^*)\sin x^*\, dx^*$$

$$= \frac{1}{4\pi}(1-\alpha P\cos x^*)\left[1 + V_t\, S(\theta,E)\,(\hat{n}\cdot\hat{V}_t)\right]\sin x^* dx^* d\phi$$

$$= \frac{1}{4\pi}(1-\alpha P\cos x^*)\left\{1 + S(\theta,E)\left[(\hat{k}_i\times\vec{V})\times\hat{k}_i\right]\cdot\hat{n}\right\}\sin x^* dx^* d\phi$$

VI. EXPERIMENTAL RESULTS

6.1 General Properties of the Λ^0 Sample

There were 741 Λ^0 hyperons, decaying via the mode

$$\Lambda^0 \longrightarrow p + \pi^-$$

in the pictures from 0 to 160,000 and satisfying the criteria of Chapter III. Only the pictures from 0 to 140,000 were used for the decay distribution studies as all possible events were measured in these. These pictures contained 645 Λ^0 decays that had a coplanarity angle of less than seven degrees and Λ^0 flight length before decay of greater than .5 cm. Of these, 222 were associated with a K_1^0 meson as identified under the rules set forth in Chapter III. 60 decays were associated with K_1^0 mesons decaying via the mode

$$K_1^0 \longrightarrow \pi^0 + \pi^0$$

followed by the decay

$$\pi^0 \longrightarrow 2\gamma \quad .$$

This mode was detected when the γ rays were converted into electron pairs in the xenon. The identification of this decay mode was accomplished when two to four electron pairs were discovered that pointed to one small area in the xenon - that area including no particle interaction. The detailed methods of detecting this neutral decay mode have been discussed in a previous article[28].

130 Λ^0 decays were accompanied by K^+ mesons. The signature of a K^+ meson was a stopping particle, with a rapidly increasing bubble density, decaying either into three slow charged π mesons or into a single parti-

cle that traveled at least 20 cm before stopping. These criteria eliminated π^+ mesons from the K^+ sample.

The remaining 233 Λ^0 decays also came from π^- meson interactions but were associated with no visible strange particles either charged or uncharged. It was assumed that these Λ^0's were associated with the long lived K_2^0 mesons. As less than one percent of the π^- meson interactions producing associated Λ^0-K_1^0 particles produced additional charged particles that left the bubble chamber, all the interactions producing only Λ^0 hyperons were required to produce no additional particle which left the chamber.

6.2 Determination of αP

The parameter α could be determined without including the information that P is non-zero. Inspection of the expression for the proton polarization given in 5.1 shows that inclusion of the Λ^0 polarization, P, and the product αP, increases the weighting of the events. For example, if $\alpha P = .38$ and this information is included in the analysis of the scatterings, the error in the results would be reduced to 84% if the error evident when $\alpha P = 0$. As P cannot be determined before performing the scattering analysis, P was replaced by

$$\frac{\alpha P}{\alpha} = \frac{C}{\alpha}$$

where αP is considered to be a constant, $\alpha P = C$. αP was measured for the three event categories.

The proton angular distribution with respect to the direction

$$\frac{\hat{k}_B \times \hat{k}_\Lambda}{|\hat{k}_B \times \hat{k}_\Lambda|}$$

was measured for Λ^0's from Λ^0-K_1^0 production, Λ^0-K^+ production, and "unassociated" Λ^0 production. $\hat{k}_\Lambda$ is the direction of flight of the Λ^0, and $\hat{k}_B$ is the π^- beam direction. The Λ^0's from 130 Λ^0-K^+ events gave

$$C_1 = (\alpha P)_1 = .29 \pm .15$$

The Λ^0's from 286 Λ^0-K_1^0 events gave

$$C_2 = (\alpha P)_2 = .38 \pm .10$$

The Λ^0's from 233 Λ^0 events in which there was no other visible strange particle gave

$$C_3 = (\alpha P)_3 = .05 \pm .11$$

A difference between $(\alpha P)_1$ and $(\alpha P)_2$ was not surprising, but the difference between $(\alpha P)_2$ and $(\alpha P)_3$ was not expected. There is no prediction of an effect of this kind. If the difference were real, the polarization of the Λ^0 produced with K_1 mesons would be different than the polarization of the Λ^0 produced with K_2 mesons. There is a 3.5% probability that $(\alpha P)_2$ and $(\alpha P)_3$ came from the same proton distribution.

6.3 Determination of α

All the Λ^0's in the picture from 0 to 160,000 were scanned for proton scatterings. The events were grouped according to the criteria set forth in 6.1. All Λ^0 events associated with one and only one charged particle originating in the π^- beam interaction and leaving the chamber were added to the Λ^0-K^+ sample. This inclusion was based on the observation that there were no Λ^0-K^+ events that evidenced, besides the K^+ meson, a second charged particle that originated in the beam interaction and that left the chamber.

The 741 Λ^0 decays in the 160,000 pictures represented 3480 gm/cm^2 of proton track in xenon. 130 proton-nuclear scatterings were detected

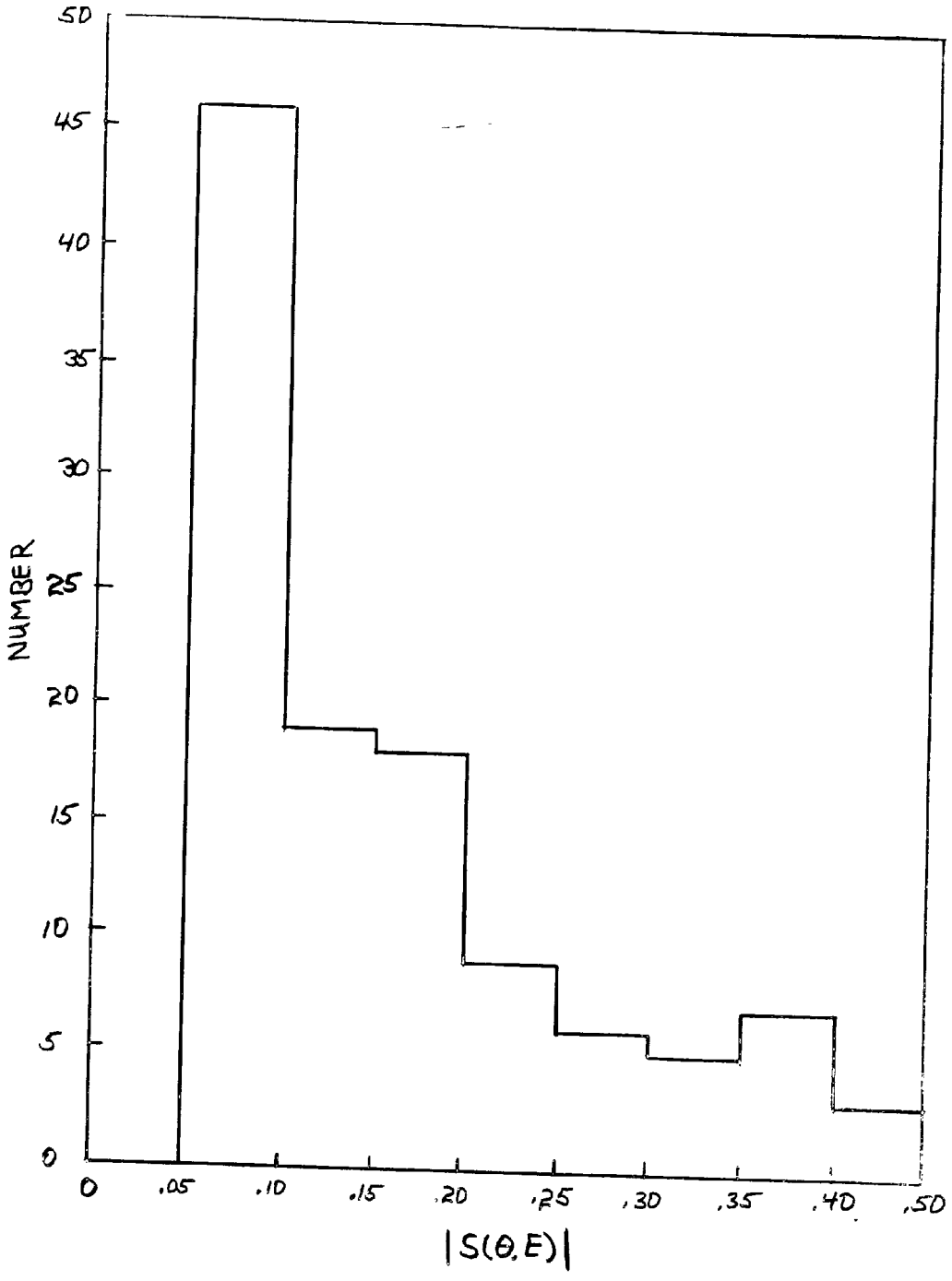


Figure 11. $|S(\theta,E)|$ Distribution (113 Events).

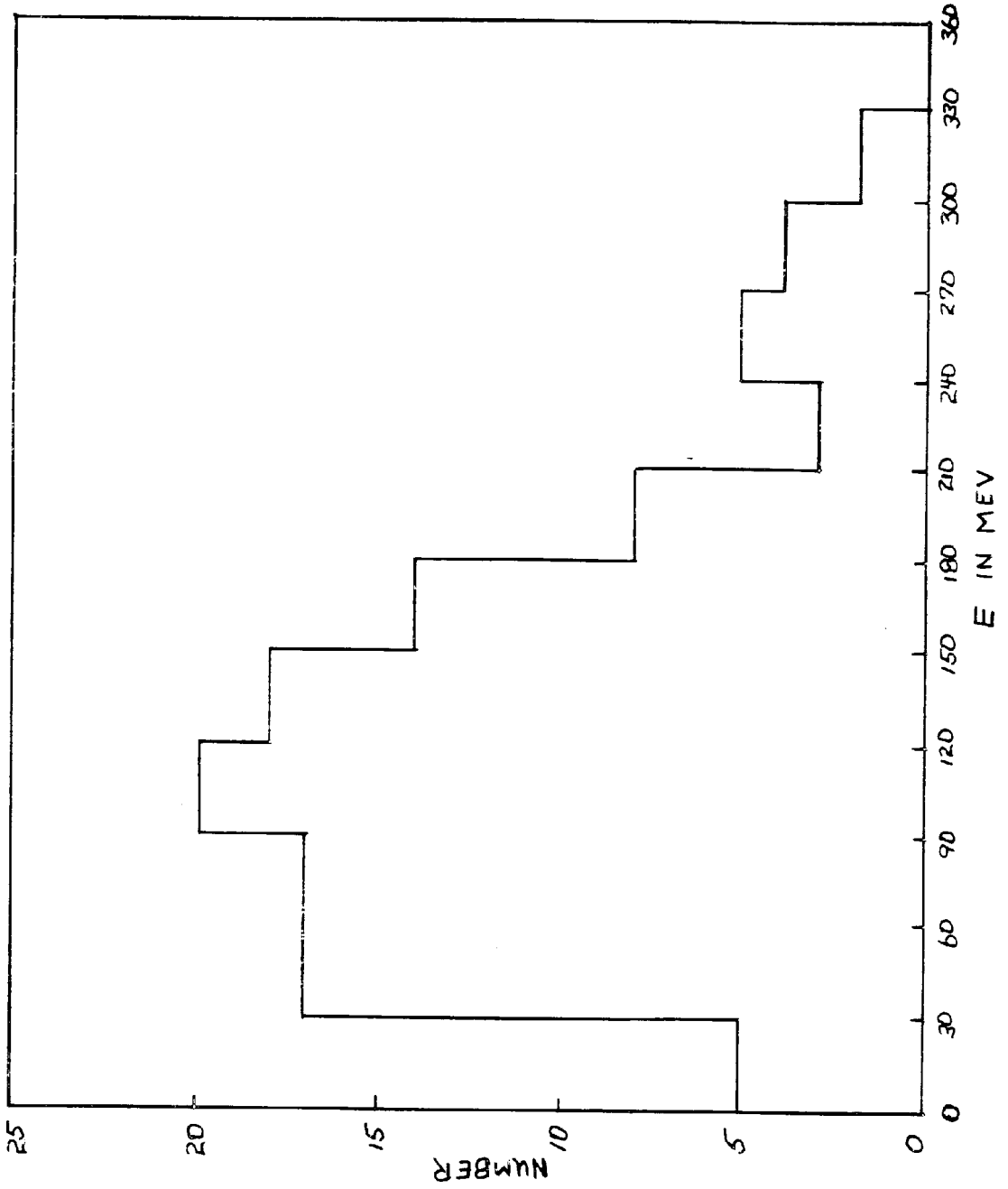


Figure 12. Distribution of Proton Energy at the Scattering (113 Events).

which had an $|S(\theta,E)| \geq .05$. Figure 11 shows the distribution of $|S(\theta,E)|$ for the scatterings with $|\Delta E| \leq 40$ MeV. Figure 12 shows the distribution of the proton energy at the scattering. Figure 13 represents the Λ^0 momentum distribution for events occurring in pictures with less than 16 beam tracks.

The statistical method used to express the experimental results was the Maximum Likelihood Method[29]. The probability of observing a particular event configuration in the scattering sample is

$$P_j(x^*,\phi)\sin x^* \, dx^* \, d\phi =$$

$$\frac{1}{4\pi}(1-\alpha P\cos x^*)\left\{1+S(\theta,E)\left[(\hat{k}_i \times \hat{k}_p^*)\times \hat{k}_i\right]\cdot \hat{n}\right\}$$

$$\times \sin x^* \, dx^* \, d\phi$$

as shown in 5.3. The Likelihood Function, $L(\alpha)$ is defined by

$$\mathcal{L}(\alpha) = \prod_{j=1}^{N} P_j$$

When $L(\alpha)$ is plotted against the parameter to be measured, α, the value of the parameter at $\frac{\partial \mathcal{L}}{\partial \alpha} = 0$ is the most probable value.

In the Appendix 8.2 it is shown that it is possible to measure the three parameters, α, β, and γ independently, if the Λ^0 decays associated with proton scatterings are uniformly distributed in the angle, ν^*, and if the protons from these Λ^0 decays had the measured distribution,

$$f(x^*) = \frac{1}{2}(1-\alpha P\cos x^*) \, .$$

Figure 14 represents the distribution in ν^* of the 130 scattering events with $|S(\theta,E)| \geq .05$. A χ^2 test indicated that there was 30%

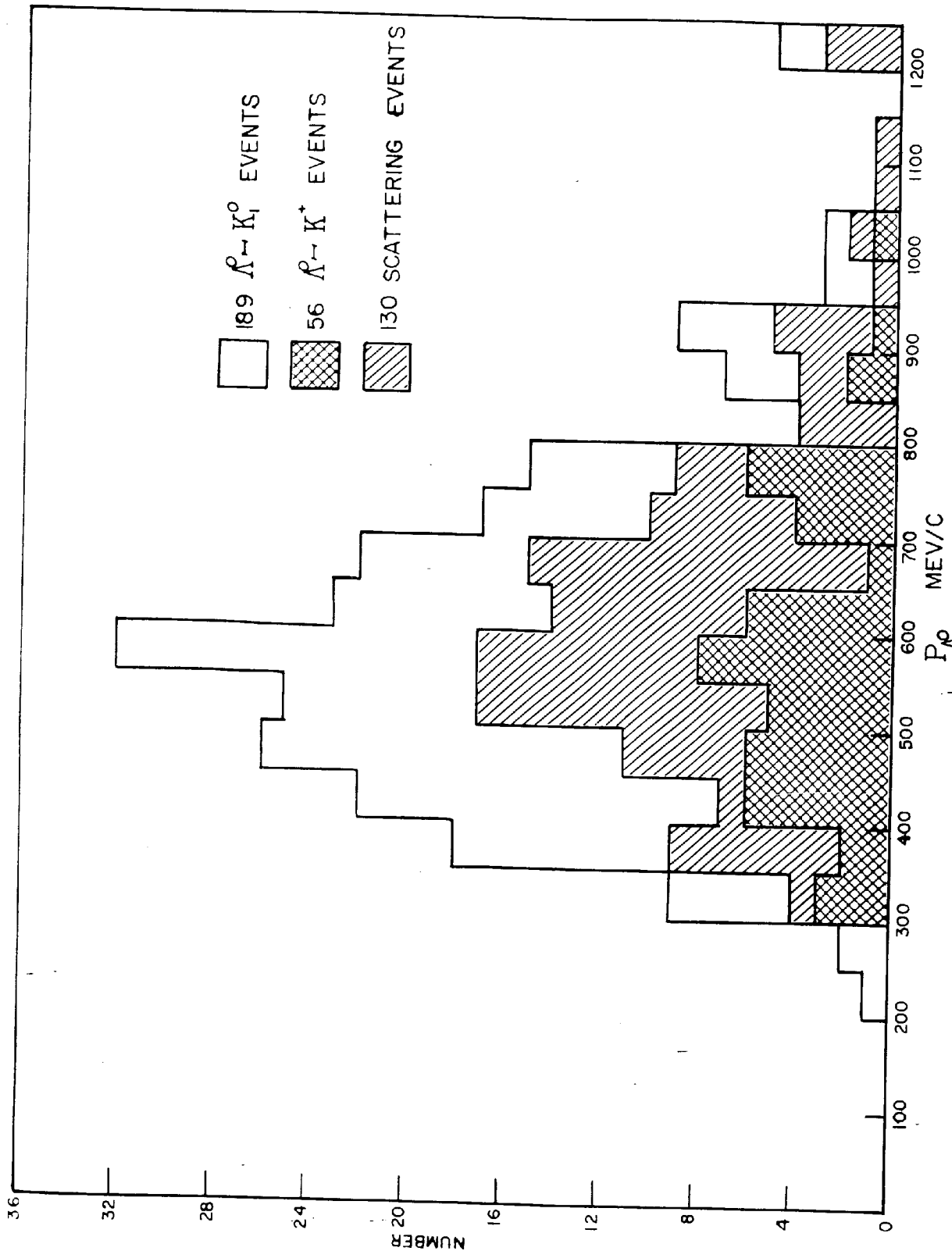


Figure 13. Λ^0 Momentum Distributions

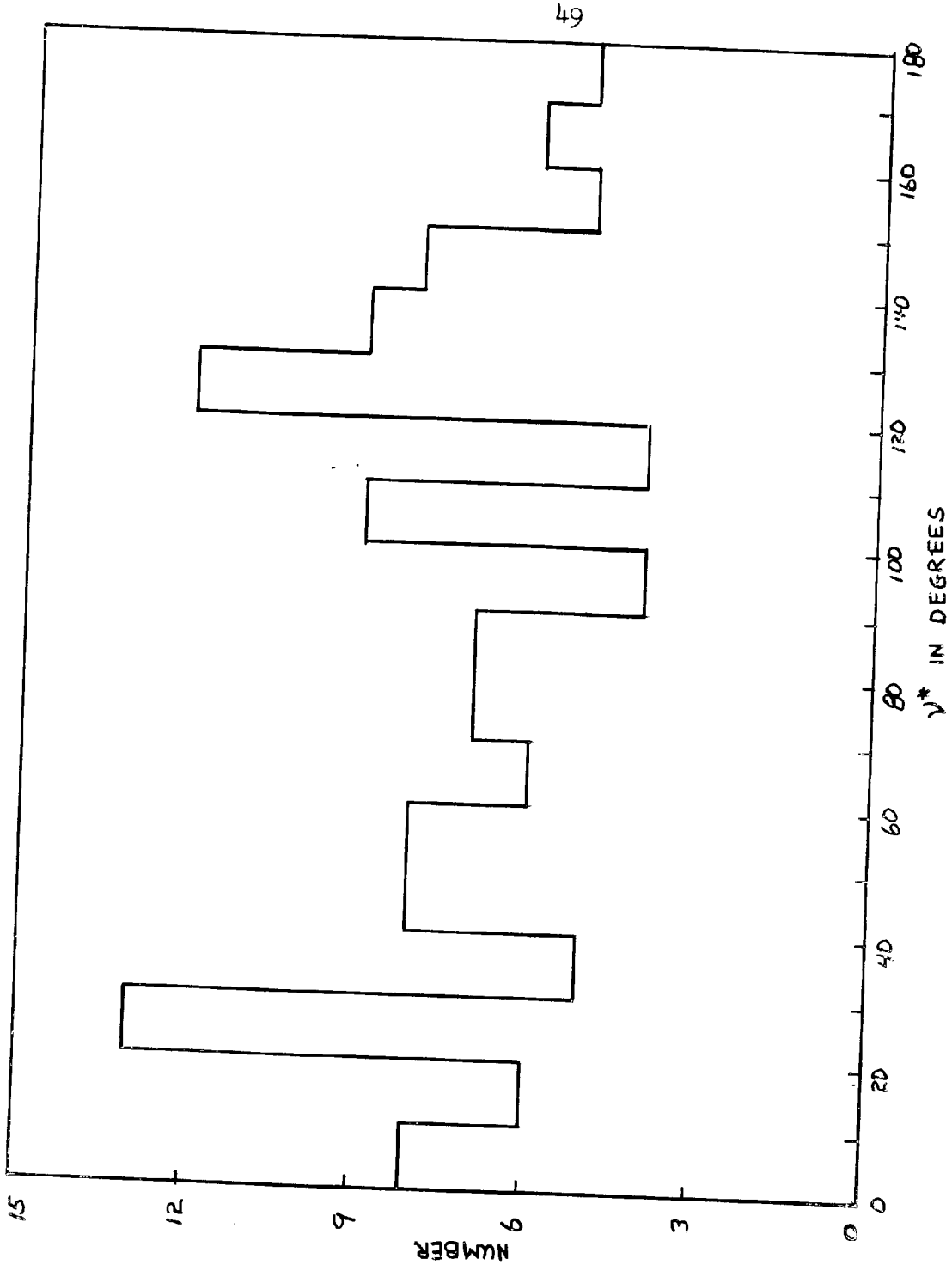


Figure 14. ν^* Distribution (130 Events).

probability that the plotted distribution arose from a uniform one. As the 130 scattering events were included in the samples used to measure the αP values for the Λ^0- K_1^0, Λ^0-K^+, and Λ^0- K_2^0 production modes, they were assumed to have had the same proton distribution as the larger sample from which they came. Any measurement of the αP values using only the events containing proton scatterings would have been meaningless because of the large statistical errors.

In this analysis αP was considered to be a constant for each of the three event type groups.

$$C_i = (\alpha P)_i$$
$$i = 1, 2, 3$$

Thus p was written

$$p(x^*, \phi) =$$

$$\frac{1}{4\pi}(1 - C\cos x^*)\left\{1 + S(\theta, E)\frac{-\alpha + C\cos x^*}{1 - C\cos x^*}\left[(\hat{k}_i \times \hat{k}_p^*) \times \hat{k}_i\right] \cdot \hat{n}\right\}$$

where

$$\cos\phi = \frac{\left[(\hat{k}_i \times \hat{k}_p^*) \times \hat{k}_i\right] \cdot \hat{n}}{|\hat{k}_i \times \hat{k}_p|}$$

and

$$\hat{n} = \frac{\hat{k}_i \times \hat{k}_f}{|\hat{k}_i \times \hat{k}_f|}$$

$\hat{n}$ is the normal to the scattering plane. This expression was simplified, giving

$$P(\chi^*, \phi) = \frac{1}{4\pi}\left\{1 - c\cos\chi^* + S(\theta,E)(-\alpha + \tfrac{5}{2}\cos\chi^*)(\hat{k}_p^* \cdot \hat{n})\right\}$$

p was calculated for each scattering event - the values of $S(\theta,E)$, c_i, χ^*, $\hat{k}_p^*$, and $\hat{n}$ inserted in the expression. The product of all the p's was the function of $L(\alpha)$. $L(\alpha)$ was calculated for 113 scattering events that had $|S(\theta,E)| \geq .05$ and $|\Delta E| \leq 40$ MeV, and is shown in Figure 15. The region between $\alpha = -.38$ and $\alpha = +.38$ is a non-physical region where α is less than αP; that is, the polarization of the Λ^0 sample, P, is greater than one - a physical impossibility.

Crawford, et al.[30], reported a lower limit for $|\alpha|$ of

$$|\alpha| \geq .73 \pm .14$$

The ratio of the area under $L(\alpha)$ between $\alpha = -.73$ and $\alpha = -1.00$ to the area under $L(\alpha)$ between $\alpha = +.73$ and $\alpha = +1.00$ is 3.2:1. The ratio of the area under $L(\alpha)$ between $\alpha = -.59$ and $\alpha = -1.00$ to the area under $L(\alpha)$ between $\alpha = +.59$ and $\alpha = +1.00$ is 3.5:1. Thus, the probability that α is negative is approximately 77%.

6.4 Discussion of the Result

The determination that the sign of α is negative disagrees with sign of α found by Boldt, et al.[31]. A negative sign is also in disagreement with the sign predicted by V-A theory[32]. The sign of α as determined by this experiment is in agreement, however, with that found by Birge[33]. Birge found

$$\alpha = -.45 \pm .40$$

Unfortunately, the present experiment does not contain sufficient information to decide with certainty whether Boldt or Birge found the correct result.

The absence of large amounts of observable asymmetric scattering

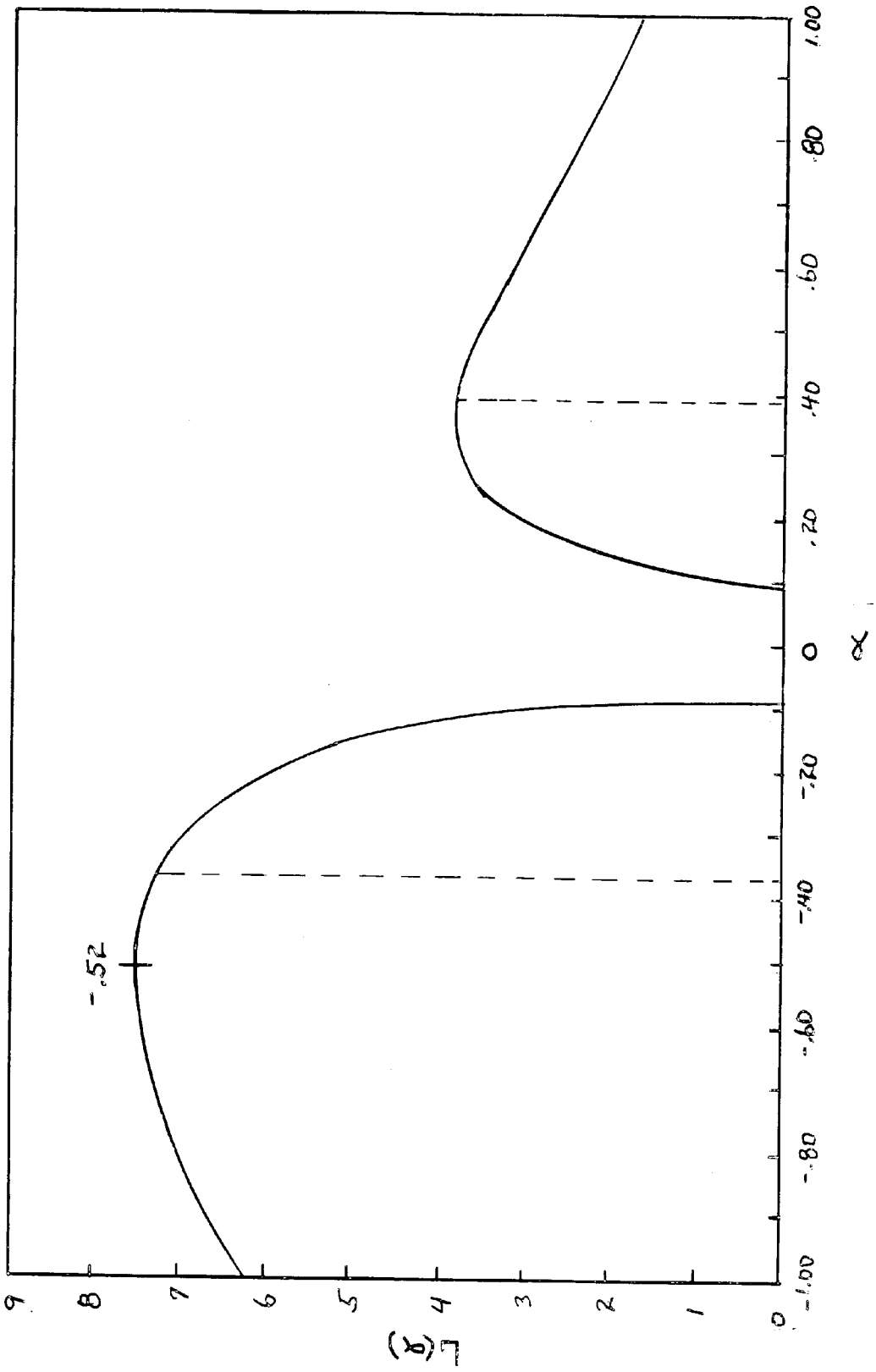


Figure 15. Likelihood Function (113 Events, $|S(\theta,E)| \geq .05$)

of the protons by xenon nuclei is evident in the distribution of the scattering events with respect to ϕ. (See Figure 16.) ϕ is defined by

$$\cos\phi = \hat{n} \cdot \hat{V}_t$$

where $\hat{n}$ is the normal to the scattering plane and $\vec{V}_t$ is the transverse polarization of the proton.

Possible causes for the lack of asymmetric scattering are incorrect values for $S(\theta,E)$, inclusion of inelastic events, and inaccurate determination of $\hat{n}$. It is difficult to believe that construction of the $S(\theta,E)$ map (Figures 7 and 8) is much in error, especially for proton scattering energies greater than 120 MeV where good data on silver were available. Only with measurement of the asymmetric scattering of protons on xenon can the $S(\theta,E)$ map be checked.

Inaccurate determination of $\hat{n}$, the normal to the scattering plan, for each scattering provides a more plausible explanation for the lack of asymmetry in ϕ. 76 of the 113 events with $|S(\theta,E)| \geq .05$ had scattering angles, θ, of less than 10 degrees. The determination of the scattering plane for such small scattering angles is the sensitive to small changes in the vectors defining the plane. 28 of the 130 scatterings were remeasured to determine the effect of measuring errors on the direction of the normal to the scattering plane. It was found that ϕ could be measured to $\pm 20^{\circ}$. Multiple scattering errors, when one centimeter track lengths are used to measure a scattering, give the same order of error in ϕ for protons scattering at an energy of approximately 140 MeV.

The inclusion of scatterings accompanied by energy loss of 20 MeV

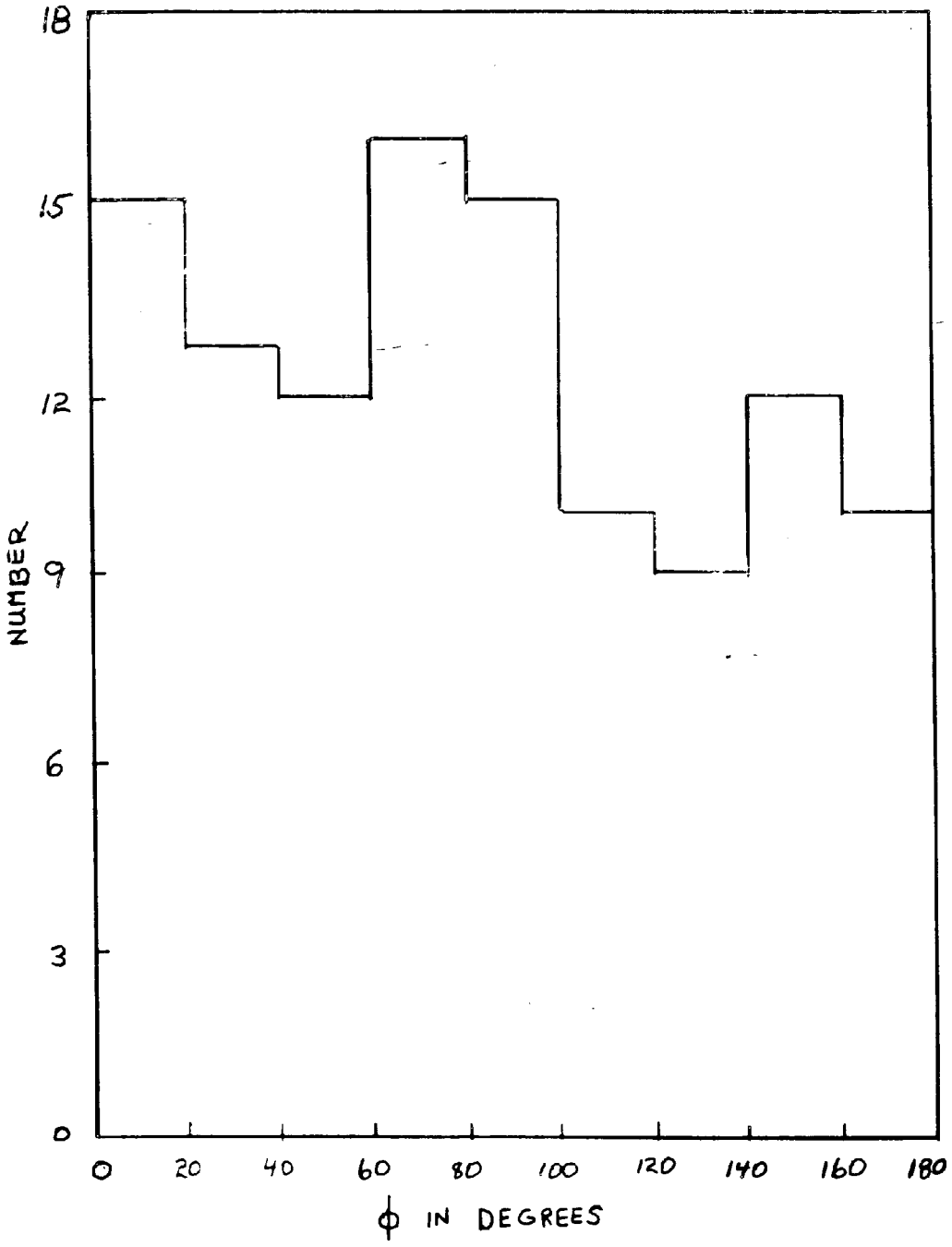


Figure 16. ϕ Distribution (113 Events).

or greater could explain the lack of asymmetry in the ϕ distribution. It was estimated in 4.3 that 28 of the 113 events used the determination of α were elastic by 20 MeV. As these scatterings show no correlation between the scattering plane and the proton polarization, they would contribute a uniform background to the ϕ distribution. However, these inelastic scatterings could seriously disrupt the determination of α if they had a scattering angle, θ, and energy, E, such that a few of them would be heavily weighted. Birge[33] found that the scatterings in his sample, that could be definitely determined to be inelastic by 20 MeV, had a large effect on his result when they were included with the elastic events. Unfortunately in this experiment, the angular inaccuracies in determining θ_π and θ_p, due to multiple scattering, did not allow a clean separation of the inelastic and elastic scatterings. Thus the effect of the inelastic events could not be checked.

Therefore, it appears that the advantage of xenon's large proton scattering cross section is offset to a great extent by the errors introduced by xenon's large Z, which governs the amount of multiple coulomb scattering experienced by charged particles.

VII. PROPOSAL FOR A NEW EXPERIMENT

7.1 Basic Considerations

It is assumed that all three Λ^0 decay parameters are to be measured. The expression for the proton polarization,

$$\vec{V} = \frac{1}{1-\alpha P\cos\chi^*}\left\{(-\alpha+P\cos\chi^*)\hat{k}^*_p+\beta P(\hat{k}^*_p\times\hat{z})\right.$$
$$\left.+\gamma P(\hat{k}^*_p\times\hat{z})\times\hat{k}^*_p\right\}$$

derived in Appendix 8.1, shows that neither the β nor the γ term can be measured if the Λ^0's are unpolarized. The first requirement for a new experiment would then be that the Λ^0's be highly polarized.

The second requirement would be that the Λ^0 momentum be as high as possible consistent with obtaining polarized Λ^0's. The high momentum would insure a high average proton momentum. A high proton momentum would minimize multiple coulomb scattering errors and maximize the analysing strength for a given scattering.

The third requirement would be that the inaccuracies in the measurement of the decay angles be small enough so that the proton energy at decay can be determined to within $\pm$ 5 MeV.

The proton energy after the scattering should be determined to within $\pm$ 5 MeV so that the energy loss at the scattering in any given event can be determined to less than 15 MeV.

The fourth requirement would be that the scattering element have a large analysing strength, $S(\theta,E)$, for a large range of proton energies. The element should also have a reasonably short nuclear scattering mean-free-path.

These four requirements will now be discussed in detail.

7.2 Polarization Requirement

As indicated in the previous section it is necessary to have a polarized Λ^0 sample to measure β and γ. In fact, the higher the polarization the more information there will be in the scatterings. An $\alpha P = .38$ decreases the error in a measurement of α to 84% of the error found when an unpolarized Λ^0 sample is studied. An $\alpha P = .73$ decreases the error in a measurement of α to 65% of the error found when an unpolarized Λ^0 sample is studied. These estimates are based on the formula

$$\Delta\alpha = \left[\frac{S(\theta,E)}{2}\int_0^{2\pi} d\phi \int_0^{\pi} \sin\chi^* d\chi\, p\, \frac{\partial^2 R}{\partial \alpha^2}\right]^{-1/2}$$

found in UCRL Report 8417[34], p is the probability of finding a given configuration as defined in 5.3. R is defined by

$$R = \ln p$$

Large Λ^0 polarization can be obtained with Λ^0's produced by π mesons. No polarization has been observed in Λ^0's produced in K^- interactions. 1 GeV π^- mesons on hydrogen have produced Λ^0's with an $\alpha P = .73 \pm .14$[30], while .99 GeV π^+ mesons on deuterium have produced Λ^0's with an $\alpha P = .55 \pm .06$[35]. In the present experiment 1 GeV π^- mesons on xenon produced Λ^0's with an $\alpha P = .38 \pm .10$

An $\alpha P = .5$ does not appear to be unreasonable to expect in medium atomic weight materials. Λ^0's produced by 1.2 to 1.9 GeV π^- mesons on iron[31] were not polarized. This indicates that for a maximum effect the π energy should not be much greater than 1 GeV.

7.3 Λ^0 Momentum Requirement

It is desirable to have a high average Λ^0 momentum as this insures a high average proton momentum. From Figures 7 and 8 it can be seen that high analysing strengths occur at small scattering angles for proton energies greater than 140 MeV. This effect is characteristic of all materials.

In this experiment the average Λ^0 momentum was approximately 600 MeV/c. (See Figure 12.) However, 63% of the scatterings occurred at a proton energy of less than 140 MeV. Most of the low energy scatterings came from protons with low inital energies since fast protons left the chamber in most cases.

Figure 17 shows the product of $S(\Theta,E)$ multiplied by the differential cross section as a function of scattering angle and energy. It again indicates the importance of scatterings at proton energies near 140 MeV. It can be seen that if $S(\Theta,E)$ is well known for proton energies near 100 MeV, the scatterings at this energy will add substantially to the information in the experiement.

7.4 Requirement on Energy Loss Measurement

Any scattering which is accompanied by an energy loss of 15 MeV or greater shows no correlation between the normal to the scattering plane and the proton polarization vector[23]. Birge[33] found that these inelastic events had a large effect on his result. In an accurate de-

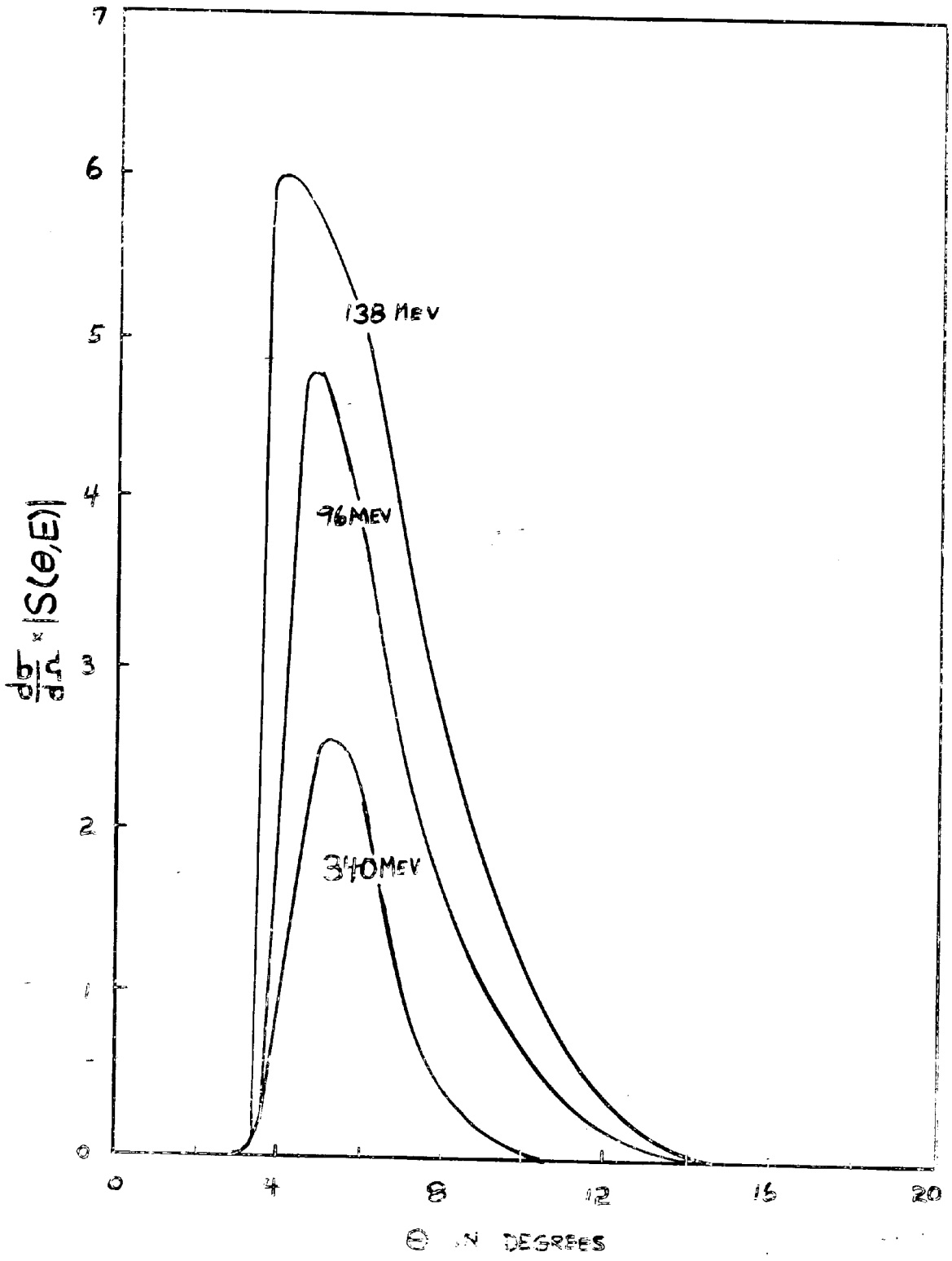


Figure 17. $\frac{d\sigma}{d\Omega} \times |S(\theta,E)|$ as Function of θ.

termination of the Λ^0 decay parameters, their influence must be eliminated. To eliminate these inelastic events it is necessary to determine the energy of the proton before and after the scattering with an accuracy great enough to detect an energy loss of 15 MeV at the scattering.

The initial proton energy can be determined if the momentum of the decay pion and the total opening angle of the Λ^0 are known. However, the proton energy is relatively insensitive to small changes in the opening angle. The initial proton energy can also be determined from the opening angle and the angle between the Λ^0 flight path and the proton. This method is extremely sensitive to small changes in the Λ^0-proton angle. It is estimated that this angle would have to be determined to within one degree. Such a requirement is near the limit of present day bubble chamber techniques even when multiple scattering is much less than one degree over one cm of track length. Given a proton at 100 MeV, the radiation length of the chamber media must be greater than 100 cm if it is desired that the mean projected scattering angle be $\leq 5^{\circ}$[12]. The initial proton energy could be measured in a third way when the chamber is in a magnetic field of sufficient intensity so that the proton energy could be determined before scattering.

The proton energy after the scattering can be determined from either the residual range of the particle of the curvature of the track in a magnetic field. In order that a 300 MeV proton would stop in a medium atomic weight material, its dimensions would have to be on the order of two to three times the stopping length of 60 gm/cm^2. The proton energy could also be determined with the use of a magnetic field, but the ac-

curacy of an individual measurement would depend, to a great extent, on the orientation of the track with respect to the field.

7.5 Analysing Strength Requirement

The higher the analysing strength for a given scattering the more information it contains. At a given scattering angle and energy, the analysing strength of the elements with an atomic number less than 50 is almost twice that for xenon. However, the scattering cross sections for the lighter elements is much less than that for xenon. The product $S(\theta,E)$ times the differential scattering cross section is independent of the scattering material to first approximation. The inherent information in each scattering is thus relatively independent of the scattering material if measuring accuracies are <u>not</u> considered. The important considerations are therefore ones of measuring accuracy, number of events desired, and proton energy.

7.6 Possible Experimental Methods for Determining the Λ^0 Decay Parameters

Two detection methods in use at present could be applied to the problem of determining the parameters: bubble chamgers and counters. Counter techniques involving spark chambers have the advantage of collecting large numbers of events in a relatively short time. However, the inability to measure energy loss at the scatterings would mean that the acceptable scattering angle must fall in a narrow angular region between four degrees and seven degrees. Even with this stringent criterion, approximately ten percent of all the scatterings would be inelastic by 20 MeV. The counter method, while useful for obtaining rough measurements, would not provide a precise determination of the parameters.

The employment of a bubble chamber to measure the Λ^o decay parameters provides many advantages compared to the counter method, but one distinct disadvantage. The disadvantage is the relative rarity of the associated production process,

$$\pi + N \longrightarrow \Lambda^o + K$$

with 1 GeV incident pions.

A suitable bubble chamber liquid with a radiation length greater than 100 cm is propane. A chamber approximately two meters in length, height, and depth would provide sufficient path length for almost all protons to come to rest, if their initial energy was less than 300 MeV. The use of propane would allow measurement of the decay angles with enough precision so that the initial proton energy could be determined to within $\pm$ 5 MeV. As the size of the chamber is on the order of two times the path length of a 300 MeV proton, no magnetic field would be needed - the residual range measurements determining the energy of the proton after the scattering. The absence of a magnetic field would allow the use of a glass rod in scanning for scattering. This method has proven exceptionally good in the present experiment. The method is described in 3.3.

The analysing strength of carbon in well known[15, 19, 24]. It is great even at small scattering angles. From the proton-carbon scattering cross section, it is estimated that one proton out of 25 would scatter at a useful angle and energy. If there were one Λ^o decay in every 20 pictures, the number of useful events would be two per 1000 pictures. At this rate, it is estimated that 5×10^5 pictures would be required to measure α to an accuracy of $\pm$ .12. This estimate is

based on Birge's measurement of α in a propane bubble chamber[33] and includes the accuracy gained from using a polarized Λ^0 sample, which he did not have.

The bubble chamber method of measuring the Λ^0 decay parameters is an accurate method, but it involves a massive effort. Yet, it appears to be the best method available at present.

VIII. APPENDICES

8.1 Derivation of the Angular Distribution and Polarization of the Protons from Λ^0 Hyperons

Consider a coordinate system for each Λ^0 decay that is defined by

$$\hat{z} = \frac{\hat{k}_B \times \hat{k}_\Lambda}{|\hat{k}_B \times \hat{k}_\Lambda|}$$

$$\hat{y} = \hat{k}_\Lambda$$

$$\hat{x} = \hat{y} \times \hat{z}$$

where $\hat{k}_B$ is a unit vector in the direction of the π^- meson which produced the Λ^0 hyperon and $\hat{k}_\Lambda$ is a unit vector in the Λ^0 flight direction. This coordinate system is show in Figure 10. Assume that the Λ^0's are completely polarized in the $\hat{z}$ direction, i.e., the expectation value of the Λ^0 spin is one in the $\hat{z}$ direction and zero in the $\hat{x}$ and $\hat{y}$ directions.

Now consider a new coordinate system defined so that

$$\hat{z}' = \hat{k}_p^*$$

$$\hat{y}' = \frac{\hat{k}_p^* \times \hat{z}}{|\hat{k}_p^* \times \hat{z}|}$$

$$\hat{x} = \hat{y} \times \hat{z}$$

where $\hat{k}_p^*$ is the direction of the decay proton in the Λ^0 rest frame. The Λ^0 spin wave function can then be described in terms of a linear combination of spin along $\hat{z}$ and spin along $-\hat{z}$ wave functions.

$$\Lambda^0 = a\rho + b\varsigma$$

ρ and ς are the final state wave functions (ignoring final state interactions) for the spin along $\hat{z}'$ and the spin along $-\hat{z}$ cases respectively, while a and b are the complex amplitudes of the two possibilities.

The components of the Λ^0 polarization in the primed coordinate system ($\hat{x}'$, $\hat{y}'$, $\hat{z}'$) are the expectation values of the Λ^0 spin along the coordinate axes.

$$P_{x'} = \langle \sigma_{x'} \rangle = \frac{2\,\mathrm{Re}\, a^+ b}{a^2 + b^2}$$

$$P_{y'} = \langle \sigma_{y'} \rangle = \frac{2\,\mathrm{Im}\, a^+ b}{a^2 + b^2}$$

$$P_{z'} = \langle \sigma_{z'} \rangle = \frac{a^2 - b^2}{a^2 + b^2}$$

a^+ is the complex conjugate of a. Note also that $P_{z'} = \hat{z} \cdot \hat{k}_p^* = \cos\theta^*$, and that $P_{y'} = 0$.

The spin wave functions, ρ, and ς, can be expressed in terms of the vector sums of the proton spins in the $\hat{z}$ and $-\hat{z}$ directions, since angular momentum is assumed to be conserved in the decay. Using the Clebsch-Gordon coefficients[27], the following expressions are obtained:

$$p = A Y_0^0 \eta + B\left(-\sqrt{\tfrac{2}{3}}\, Y_1^1 \mu - \sqrt{\tfrac{1}{3}}\, Y_1^0 \eta\right)$$

$$n = A Y_0^0 \mu + B\left(\sqrt{\tfrac{1}{3}}\, Y_1^0 \mu - \sqrt{\tfrac{2}{3}}\, Y_1^{-1} \eta\right).$$

η represents the proton spin wave function for the proton spin along $\hat{z}$; μ, the proton spin wave function for the proton spin along $-\hat{z}$. A is the complex amplitude of the S angular momentum waves in the decay, and B is the complex amplitude of the P angular momentum waves in the decay. The Y's are the spherical harmonics which characterize the orbital angular momentum spectrum of the decay. In general

$$Y_0^0 = \frac{1}{\sqrt{4\pi}}$$

$$Y_1^0 = \sqrt{\frac{3}{4\pi}} \cos\chi'$$

$$Y_1^1 = -\sqrt{\frac{3}{8\pi}} \sin\chi' e^{-i\phi'}$$

$$Y_1^{-1} = \sqrt{\frac{3}{8\pi}} \sin\chi' e^{-i\phi'}$$

where the angles χ' and ϕ' are respectively the polar and azimuthal angles of the proton in the Λ^0 rest frame with respect to the $\hat{x}'$, $\hat{y}'$, $\hat{z}'$ coordinate system. Note that $\hat{z}' = \hat{k}_p^*$, $\chi' = 0$. Thus,

$$p = (A - B)\eta$$

$$n = (A + B)\mu,$$

and

$$\Lambda^0 = a(A - B)\eta + b(A + B)\mu.$$

Next it is necessary to find the proton polarization in the primed coordinate system; that is, the expectation values of the proton spin along $\hat{x}'$, $\hat{y}'$, $\hat{z}'$ axes.

$$V_{z'} = \frac{a^2(A-B)^2 - b^2(A+B)^2}{a^2(A-B)^2 + b^2(A+B)^2}$$

$$= \frac{-\alpha + \cos x^*}{1 - \alpha \cos x^*}$$

where

$$\alpha = \frac{2 \mathrm{Re}\, A^+ B}{A^2 + B^2}$$

$$\cos x^* = P_{z'} = \frac{a^2 - b^2}{a^2 + b^2} .$$

$$V_{y'} = \frac{2 \mathrm{Im}[a^+(A^+ - B^+) b (A+B)]}{(1 - \alpha P_{z'})(a^2 + b^2)(A^2 + B^2)}$$

$$= \frac{\beta \sin x^*}{1 - \alpha \cos x^*}$$

where $$\beta = \frac{2\,\mathrm{Im}\,A^{+}B}{A^2 + B^2}$$

$$P_{x'} = \frac{2\,\mathrm{Re}\,a^{+}b}{a^2 + b^2} = \sin x^{*} .$$

$$V_{x'} = \frac{2\,\mathrm{Re}\left[a^{+}(A^{+} - B^{+})\,b\,(A + B)\right]}{(1 - \alpha P_{y'})(a^2 + b^2)(A^2 + B^2)}$$

$$= \frac{\gamma \sin x^{*}}{1 - \alpha \cos x^{*}}$$

where $$\gamma = \frac{A^2 - B^2}{A^2 + B^2} .$$

From these components, the proton polarization vector, $\vec{V}$, is formed

$$\vec{V} = \frac{1}{1 - \alpha \cos x^{*}} \left\{ (-\alpha + \cos x^{*})\,\hat{k}_p^{*} + \beta(\hat{k}_p^{*} \times \hat{z}) \right.$$

$$\left. + \gamma\left[(\hat{k}_p^{*} \times \hat{z}) \times \hat{k}_p^{*}\right] \right\} .$$

This is the expression for $\vec{V}$ if the Λ^{0} is completely polarized in the $\hat{z}$ direction.

For an incompletely polarized Λ^{0} sample, the beam is an incoherent

mixture of spin-up (along $\hat{z}$) and spin-down (along $-\hat{z}$) Λ^0 wave functions. If U^2 is the probability that the Λ^0 spin is up, and D^2 is the probability that the Λ^0 spin is down, then the polarization of the Λ^0 sample is

$$P = \frac{U^2 - D^2}{U^2 + D^2} .$$

The decay distribution of the protons from the Λ^0's with spin up is

$$I_{up} = \sum_{\substack{\text{PROTON} \\ \text{SPIN}}} |\rho|^2 = (1 - \alpha \cos x^*)$$

while the distribution for Λ^0's with the spin down is

$$I_{DOWN} = \sum_{\substack{\text{PROTON} \\ \text{SPIN}}} |\xi|^2 = (1 + \alpha \cos x^*)$$

and for a partially polarized Λ^0 sample is

$$I = \frac{U^2 I_{up} + D^2 I_{DOWN}}{U^2 + D^2}$$

$$= 1 - \alpha P \cos x^*$$

To find the proton polarization when the Λ^0's are partially polarized, it is necessary to multiply the probability that the Λ^0 spin is up by the proton polarization for spin-up and to add this to the probability that the Λ^0 spin is down multiplied by the proton polarization for Λ^0 spin-down:

$$\vec{V}_{ave} = \frac{U^2}{U^2+D^2}\,\vec{V}(x^*) + \frac{D^2}{U^2+D^2}\,\vec{V}(-x^*) .$$

Working out the 'z' component

$$V_z = \frac{U^2(-\alpha+\cos x^*)}{(U^2+D^2)(1-\alpha\cos x^*)} + \frac{D^2(-\alpha-\cos x^*)}{(U^2+D^2)(1+\alpha\cos x^*)}$$

$$= \frac{-(U^2+D^2)\alpha + (U^2-D^2)\cos x^*}{(U^2+D^2) - (U^2-D^2)\cos x^*}$$

$$= \frac{-\alpha + P\cos x^*}{1-\alpha P\cos x^*}$$

where

$$P = \frac{U^2-D^2}{U^2+D^2}$$

is the polarization of the Λ^0 sample. The other components behave similarly, giving

$$\vec{V} = \frac{1}{1-\alpha P\cos x^*}\left\{(-\alpha+P\cos x^*)\hat{k}_p^* + \beta P(\hat{k}_p^*\times\hat{z}) + \gamma P\left[(\hat{k}_p^*\times\hat{z})\times\hat{k}_p^*\right]\right\} .$$

8.2 An Analysis Theorem

The question arises whether or not it is possible to determine the three parameters, α, β, and γ, independently. To show that it is possible to determine them separately, it is necessary to prove that the transverse component of the proton polarization arising from one of the parameters has a zero average value when projected on the transverse components arising from the other two parameters, when the average is taken over an unbiased sample of Λ^0 decays.

The proton polarization vector is

$$\vec{V} = \frac{1}{1-\alpha P\cos x^*}\left\{(-\alpha + P\cos x^*)\,\hat{k}_p^* + \beta P(\hat{k}_p^* \times \hat{z}) + \gamma P\left[(\hat{k}_p^* \times \hat{z}) \times \hat{k}_p^*\right]\right\}.$$

The transverse components of the polarization are found by

$$\vec{V}_t = (\hat{k}_p \times \vec{V}) \times \hat{k}_p \,;$$

so that the transverse components from the β and γ terms are

$$\vec{V}_{\beta t} = V_\beta\left[\hat{k}_p \times (\hat{k}_p^* \times \hat{z})\right] \times \hat{k}_p$$

$$\vec{V}_{\gamma t} = V_\gamma\left[\hat{k}_p \times \left[(\hat{k}_p^* \times \hat{z}) \times \hat{k}_p^*\right]\right] \times \hat{k}_p$$

First, it is necessary to show that $\langle \hat{V}_{\beta t} \cdot \hat{V}_{\gamma t} \rangle = 0$ when averaged over the sample of Λ^0 decays.

$$\hat{V}_{\beta t} \cdot \hat{V}_{\gamma t} = (\hat{k}_p^* \times \hat{k}_p \cdot \hat{z}) \left[(\hat{k}_p \cdot \hat{z}) - (\hat{k}_p \cdot \hat{k}_p^*)(\hat{k}_p^* \cdot \hat{z}) \right]$$

For a given χ^*, as shown in Figure 10,

$$\hat{k}_p^* \times \hat{k}_p \cdot \hat{z} = f(\nu^*)$$

such that

$$\int_0^{2\pi} f(\nu^*) \, d\nu^* = 0$$

$\hat{k}_p^* \cdot \hat{z} \neq f(\nu^*)$, $\hat{k}_p \cdot \hat{z}$ and $(\hat{k}_p \cdot \hat{k}_p^*)$ are even functions of ν^*. Thus, for a sample of Λ^0 decays, distributed uniformly in ν^*, $\langle \hat{V}_{\alpha t} \cdot \hat{V}_{\beta t} \rangle = 0$.

Second, it is necessary to show that $\langle \hat{V}_{\alpha t} \cdot \hat{V}_{\beta t} \rangle = 0$ when averaged over a sample of Λ^0 decays.

$$(\hat{V}_{\alpha t} \cdot \hat{V}_{\beta t}) = (\hat{k}_p^* \cdot \hat{k}_p)(\hat{k}_p^* \times \hat{k}_p \cdot \hat{z})$$

For a given χ^*

$$\hat{k}_p^* \times \hat{k}_p \cdot \hat{z} = f(\nu^*)$$

such that

$$\int_0^{2\pi} f(\nu^*) \, d\nu^* = 0 \quad .$$

$\hat{k}_p^* \cdot \hat{k}_p$ is an even function of ν^*. Thus, for a sample of Λ^0 decays, uniformly distributed in ν^*, $\langle \hat{V}_{\alpha t} \cdot \hat{V}_{\beta t} \rangle = 0$.

Third, it is necessary to show that $\langle \hat{V}_{\alpha t} \cdot \hat{V}_{\gamma t} \rangle = 0$ when averaged over the sample of Λ^0 decays. $\hat{V}_{\alpha t}$ is a direction define by

$$\hat{V}_{\alpha t} = \frac{(\hat{k}_p \times \hat{k}_p^*) \times \hat{k}_p}{|\hat{k}_p \times \hat{k}_p^*|}$$

$$(\hat{V}_{\alpha t} \cdot \vec{V}_{\gamma t}) = \frac{\gamma P}{1 - \alpha P \cos\chi^*} \Big\{ (\hat{k}_p^* \cdot \hat{z}) - (\hat{k}_p^* \cdot \hat{k}_p)(\hat{k}_p \cdot \hat{z})$$

$$- (\hat{z} \cdot \hat{k}_p)(\hat{k}_p \cdot \hat{k}_p^*) + (\hat{k}_p \cdot \hat{z})(\hat{k}_p^* \cdot \hat{k}_p)$$

$$- (\hat{k}_p^* \cdot \hat{z}) + (\hat{k}_p^* \cdot \hat{k}_p)^2 (\hat{k}_p^* \cdot \hat{z})$$

$$+ (\hat{k}_p^* \cdot \hat{z})(\hat{k}_p \cdot \hat{k}_p^*) - (\hat{k}_p \cdot \hat{k}_p^*)(\hat{k}_p^* \cdot \hat{z}) \Big\}$$

If this dot product is weighted by the proton up-down distribution, $1 - \alpha P \cos\chi^*$, then

$$\int_0^{\pi} (1 - \alpha P \cos\chi^*)(\hat{V}_{\alpha t} \cdot \vec{V}_{\gamma t}) \sin\chi^* \, d\chi^* = 0$$

since both $\hat{k}_p \cdot \hat{z}$ and $\hat{k}_p^* \cdot \hat{z}$ are odd function of χ^*. Thus, for a sample of Λ^0 decays which has its decay proton distribution given by

$$I = (1 - \alpha P \cos\chi^*)$$

the weighted average of $\hat{V}_{\alpha t} \cdot \hat{V}_{\gamma t}$ is zero. The distribution, I, is just the measured distribution.

Therefore, it is possible to measure, independently, the parameters α, β, and γ if the Λ^0 decays are uniformly distributed in ν^* and have the measured proton distribution.

8.3 Construction of $\hat{k}_p^*$

$\hat{k}_p^*$, the direction of the proton in the Λ^0 rest frame, is a unit vector used so frequently in this study that the method of its construction will be given. Figure 18 represents the decay plane of the Λ^0 hyperon. The coordinate system is defined by

$$\hat{y} = \hat{k}_\Lambda$$

$$\hat{u} = \frac{(\hat{k}_\pi \times \hat{y}) \times \hat{y}}{|\hat{k}_\pi \times \hat{y}|}$$

where $\hat{k}_\Lambda$ is the Λ^0 flight direction, and $\hat{k}_\pi$ is the direction of the pi meson from the decaying Λ^0 hyperon. $\hat{k}_p$ is direction of the proton in the laboratory system. $\hat{k}_\pi^*$ is the direction of the pi meson from the decay in the Λ^0 rest frame. Notice that

$$\psi^* + \sigma^* = \pi$$

The Lorentz Transformation gives

$$k_\pi^* \cos\psi^* = \gamma_\Lambda k_\pi \cos\psi - \gamma_\Lambda \beta_\Lambda E_\pi$$

$$k_\pi^* \sin\psi^* = k_\pi \sin\psi$$

where E_π is the energy of the ceday pion in the laboratory; β_Λ is the velocity of the Λ^0 in units of c, the velocity of light; $\gamma_\Lambda = (1-\beta_\Lambda^2)^{-\frac{1}{2}}$, k_π^* and k_π are the magnitudes of the vector $\vec{k}_\pi^*$ and $\vec{k}_\pi$, respectively.

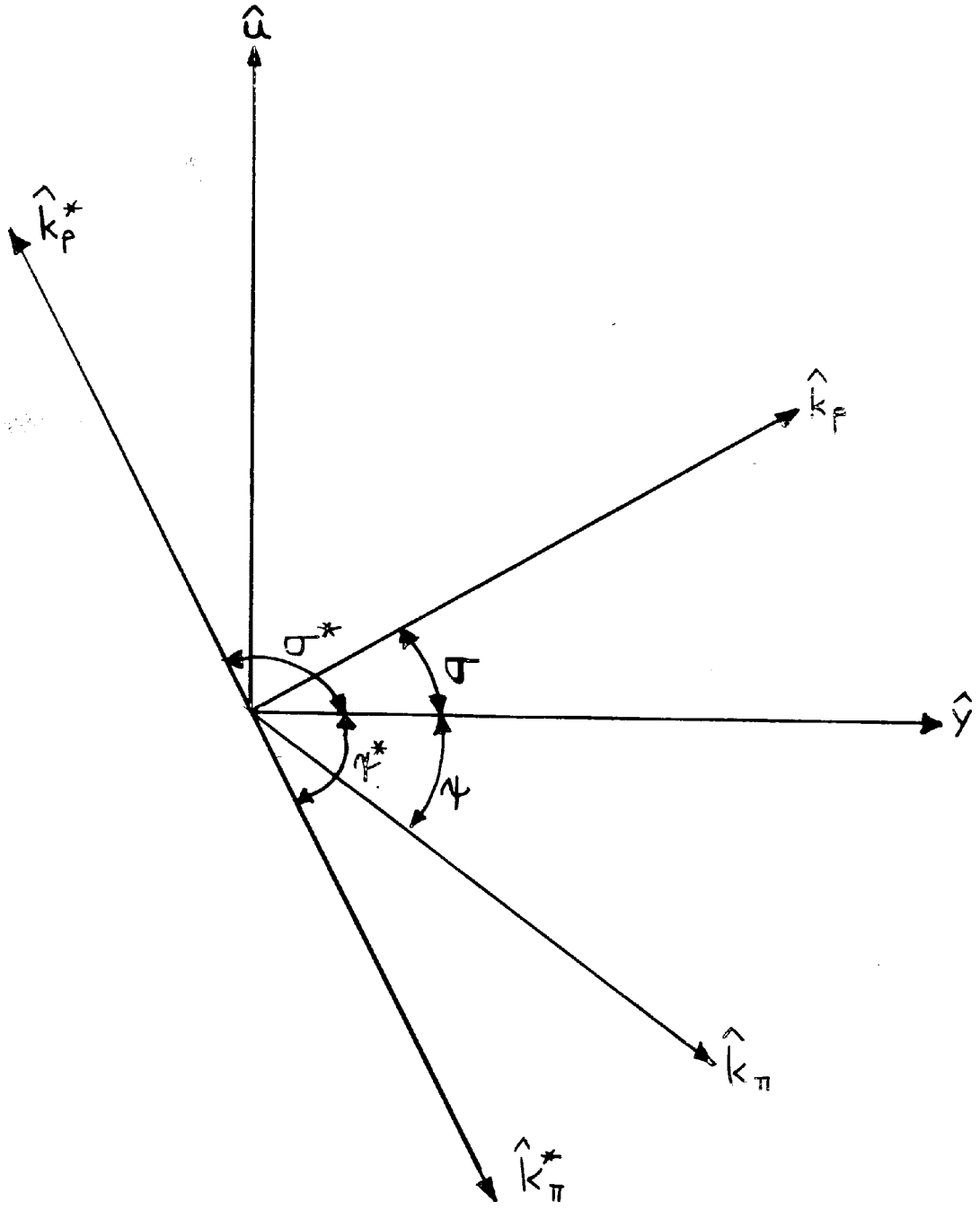


Figure 18. Coordinate System - Decay Plane.

$$\vec{k}^*_- = k^*_- \hat{k}^*_+$$

$$\vec{k}_- = k_+ \hat{k}_+$$

Calculating,

$$\tan\psi^* = \sqrt{1-\beta_1^2}\,\frac{\sin\psi}{\cos\psi - \beta_1 \frac{E_T}{k_T}}$$

Let

$$\hat{k}^*_- = R\hat{a} + T\hat{y}$$

such that

$$\tan\psi^* = -\frac{R}{T}$$

and

$$R^2 + T^2 = 1$$

Then

$$T = \frac{1}{\sqrt{1+\tan^2\psi^*}} \cdot \frac{\tan\psi^*}{|\tan\psi^*|}$$

$$R = -\frac{|\tan\psi^*|}{\sqrt{1+\tan^2\psi^*}}$$

Thus $$\hat{k}_\rho^* = -R\hat{u} - T\hat{y}$$

Or in the $\hat{x}$, $\hat{y}$, $\hat{z}$, coordinate system

$$\hat{k}_\rho^* = -R(\hat{u}\cdot\hat{x})\hat{x} - T\hat{y} - R(\hat{u}\cdot\hat{z})\hat{z}$$

Finally:

$$\cos\nu^* = -\frac{R(\hat{u}\cdot\hat{x})}{\sqrt{1-R^2(\hat{u}\cdot\hat{z})^2}}$$

LIST OF REFERENCES

1. F. S. Crawford, Jr., M. L. Good, M. Cresti, M. L. Stevenson, and H. K. Ticho, Phys. Rev. Letters 2, 114 (1959).

2. F. S. Crawford, Jr., M. Cresti, M. L. Good, F. T. Solmitz, and M. L. Stevenson, Phys. Rev. Letters 2, 11 (1959).

3. F. S. Crawford, Jr., M. Cresti, M. L. Good, K. Gottstein, E. M. Lyman, F. T. Solmitz, M. L. Stevenson, and H. K. Ticho, Phys. Rev. 108, 1102 (1957).
F. Eisler, R. Plano, A. Prodell, N. Samois, M. Schwartz, J. Steinberger, P. Bassi, V. Borelli, G. Puppi, G. Tanaka, P. Woldschek, V. Zoboli, M. Conversi, P. Franzini, I. Mannelli, R. Santangelo, B. Silverstrini, D. A. Glaser, C. Graves, and M. L. Perl, Phys. Rev. 108, 1353 (1957).

4. T. D. Lee and C. N. Yang, Phys. Rev. 108, 1645 (1957).

5. L. Wolfenstein, Annual Reviews of Nuclear Science, 6, 43 (1956).

6. D. A. Glaser, Handbuch der Physik, edited by S. Flugge (Springer-Verlag, Berlin, 1958), Vol. 45, p. 314.

7. J. L. Brown, D. Glaser, and M. Perl, Phys. Rev. 102, 586 (1956).

8. R. L. Cool, Bruce Cork, James W. Cronin, and William A. Wenzel, Phys. Rev. 114, 912 (1959).

9. R. M. Sternheimer, Phys. Rev. 115, 137 (1959).

10. M. C. Walske, Phys. Rev. 101, 940 (1956).

11. W. F. Fry and G. R. White, Phys. Rev. 93, 1427 (1954).

12. W. H. Barkas and A. H. Rosenfeld, UCRL Report 8030, 8 (1958).

13. I. E. Dayton and G. Shrank, Phys. Rev. 101, 1358 (1956).

14. G. Gerstein, J. Niederer, and K. Strauch, Phys. Rev. 108 427 (1957).

15. J. M. Dickson, Private Communication

16. R. E. Richardson, W. P. Ball, C. E. Leith, Jr., and B. J. Moyer, Phys. Rev. 86, 29 (1952).

17. J. M. Dickson, B. Rose, and D. C. salter, Proc. Phys. Soc. London, A68, 361 (1955).

18. J. Marshall and L. Marshall, Phys. Rev. 98, 1398 (1955).

19. A. Alphonce, A. Johansson, and G. Tibell, Nuclear Phys. 4, 643 (1957).

20. A. K. Kerman, H. McManus, and R. M. Thaler, Annals of Phys. 8, 551 (1959).

21. W. A. Blanpied, Phys. Rev. 113, 1099 (1959).

22. E. Heiberg, Phys. Rev. 106, 1271 (1957).

23. P. Hillman, A. Johansson, and H. Tyren, Nuclear Phys. 4, 648 (1957).

24. H. Tyren, and A. J. Maris, Nuclear Phys. 4, 637 (1957).

25. E. P. Wigner, Revs of Modern Phys. 29, 255 (1957).

26. S. Hayakawa, Phys. Rev. 108, 1533 (1957)

27. E. U. Condon and G. H. Shortly, Theory of Atomic Spectra, p. 76, (Cambridge University Press, 1957).

28. J. L. Brown, H. C. Bryant, R. A. Burnstein, R. W. Hartung, D. A. Glaser, J. A. Kadyk, D. Sinclair, G. H. Trilling, J. C. Vander Velde, and J. D. van Putten, Phys. Review Letters 3, 51 (1959).

29. M. Annis, W. Cheston, H. Primakov, Rev. Mod. Phys. 25, 818 (1953).

30. P. S. Crawford, Jr., M. Cresti, M. L. Good, K. Gottstein, E. M. Lyman, F. T. Solmitz, M. L. Stevenson, and H. K. Ticho, 1958 Annual International Conference on High Energy Physics (CERN, Scientific Information Service, Geneva, 1958) p. 323.

31. E. Boldt, H. S. Bridge, D. O. Caldwell, and Y. Pal, Phys. Rev. Letters 1, 256 (1958).

32. S. Okubo, R. E. Marshak, and E. C. G. Sudershan, Phys. Rev. 113, 944 (1959)

33. R. W. Birge, Private Communication.

34. J. Orear, UCRL 8417, 7 (1958).

35. J. W. Cronin, B. Cork, L. Kerth, W. A. Wenzel, and R. L. Cool, Bull. Am Phys. Soc. Ser. II, 5, 11 (1960) as reported at the meeting of the Am. Phys. Soc.